mathematics

MDPI

Article

Tensor-Based Uncoupled and Incomplete Multi-View Clustering

Yapeng Liu [1], Wei Guo [1], Weiyu Li [1], Jingfeng Su [1], Qianlong Zhou [1] and Shanshan Yu [2,3]*

[1] College of Electronic and Information Engineering, Southwest University, Chongqing 400715, China; pping7349@gmail.com (Y.L.); guowei123@email.swu.edu.cn (W.G.); liwy2024@email.swu.edu.cn (W.L.); sjf333@email.swu.edu.cn (J.S.); z1090132642@email.swu.edu.cn (Q.Z.)
[2] Training and Basic Education Management Office, Southwest University, Chongqing 400715, China
[3] Key Laboratory of Cyber-Physical Fusion Intelligent Computing (South-Central Minzu University), State Ethnic Affairs Commission, Wuhan 430074, China
* Correspondence: yu33@swu.edu.cn

Abstract: Multi-view clustering demonstrates strong performance in various real-world applications. However, real-world data often contain incomplete and uncoupled views. Missing views can lead to the loss of latent information, and uncoupled views create obstacles for cross-view learning. Existing methods rarely consider incomplete and uncoupled multi-view data simultaneously. To address these problems, a novel method called Tensor-based Uncoupled and Incomplete Multi-view Clustering (TUIMC) is proposed to effectively handle incomplete and uncoupled data. Specifically, the proposed method recovers missing samples in a low-dimensional feature space. Subsequently, the self-representation matrices are paired with the optimal views through permutation matrices. The coupled self-representation matrices are integrated into a third-order tensor to explore high-order information of multi-view data. An efficient algorithm is designed to solve the proposed model. Experimental results on five widely used benchmark datasets show that the proposed method exhibits superior clustering performance on incomplete and uncoupled multi-view data.

Keywords: multi-view clustering; uncoupled views; incomplete data; cross-view learning; self-representation

MSC: 68T01; 68T30

Academic Editor: Jonathan Blackledge

Received: 18 March 2025
Revised: 23 April 2025
Accepted: 29 April 2025
Published: 4 May 2025

Citation: Liu, Y.; Guo, W.; Li, W.; Su, J.; Zhou, Q.; Yu, S. Tensor-Based Uncoupled and Incomplete Multi-View Clustering. *Mathematics* **2025**, *13*, 1516. https://doi.org/10.3390/math13091516

1. Introduction

In the era of data explosion, multi-view data have gained widespread attention as an important form of information representation. Multi-view data refers to data that describe objects using multiple feature descriptors or are collected from different domains. For example, an image can be represented by features such as Scale-Invariant Feature Transform (SIFT), Histogram of Oriented Gradients (HOG), and Local Binary Pattern (LBP). Each descriptor or modality corresponds to a specific "view". This diverse representation not only enriches semantic information but also compensates for the limitations of single-view data, promoting wide applications in clustering [1–4], classification [5], and image segmentation [6].

Multi-view clustering (MVC), as an unsupervised learning method, aims to partition data into distinct clusters by leveraging consistent and complementary information from multiple views. For instance, in [7], multi-view learning is integrated with *k*-means into a unified framework. Methods like those in [8,9] utilize low-rank tensor constraints in multi-view clustering to explore high-order correlations between views. In comparison, tensor

Singular Value Decomposition (t-SVD)-based Multi-view Subspace Clustering (t-SVD-MSC) employs the tensor nuclear norm (TNN) and rotational tensor structures, achieving significant performance improvements in multi-view clustering [10]. Yang et al. [11] extend multi-view k-means to a federated setting, enabling multiple data clients to collaboratively train a unified multi-view k-means model without sharing raw data.

Traditional MVC methods generally assume that the data from all views are complete and fully coupled [12]. However, this assumption rarely holds in real-world scenarios, as data often face issues such as incompleteness and uncoupling. These problems are particularly prominent in certain fields. For example, in the medical field, where patients may not complete all tests, leading to missing data in some views. In social media, the same users may have different names or identifiers across platforms, leading to uncoupled data when collected from multiple sources.

Many methods have been developed to address incomplete multi-view clustering (IMVC). For example, Shen et al. [13] use subspace learning to recover missing instances and apply tensor learning to reconstruct similarity graphs. Additionally, Hu et al. [14] employ the $l_{2,1}$-norm to establish a consensus basis matrix, reducing the impact of missing entries. In addition to recovering missing views, some studies handle missing samples by utilizing data matrices or coupling information between views, directly learning shared representations from incomplete data.

For uncoupled multi-view clustering (UMVC), Yu et al. [15] employ non-negative matrix factorization (NMF) to explore cross-view coupling relationships through graph-based coupling terms. Similarly, Lin et al. [16] couple other views with the most reliable view through pairwise cross-view coupling learning and incorporate manifold learning to explore local structure. For incomplete and uncoupled multi-view data, Lin et al. [17] use the tensor nuclear norm on coupled and inferred self-representation matrices to explore high-order correlations of multi-view data. Currently, there are still very few clustering methods for incomplete and uncoupled multi-view data.

Although various approaches have been proposed to address incomplete or uncoupled multi-view clustering, real-world data often exhibit both issues simultaneously. Most models typically experience significantly degraded performance when dealing with such data. For methods targeting incomplete multi-view clustering, the presence of uncoupled data with unrelated information across views may mislead clustering results, leading to worse performance. On the other hand, the models in [15,16] fail to leverage the potential information from missing views and struggle to accurately explore high-order correlations between views due to missing data.

To address the limitations of existing models, we propose a novel multi-view clustering method named Tensor-based Uncoupled and Incomplete Multi-view Clustering (TUIMC). Specifically, we identify the view containing the most available information as the most reliable view and integrate cross-view learning, missing sample recovery, low-dimensional subspace learning, and tensor representation into a unified framework. A schematic diagram of the proposed model is shown in Figure 1. In summary, the primary contributions of this work are as follows:

- Unlike existing IMVC models, we integrate missing view recovery with the coupling of cross-view self-representation matrices. This approach not only uncovers the latent information of missing samples but also reduces the interference caused by uncoupled data.
- An algorithm based on the alternating direction method of multipliers (ADMM) [18] is designed to solve the proposed TUIMC. Extensive experiments are conducted on various datasets, showcasing the efficiency of the proposed model.

The remaining parts of this paper are structured as follows: Section 2 presents some notation and related works. Section 3 delineates the methodology of the proposed model. Section 4 contains the experimental results and analysis. Lastly, the conclusions are outlined in Section 5.

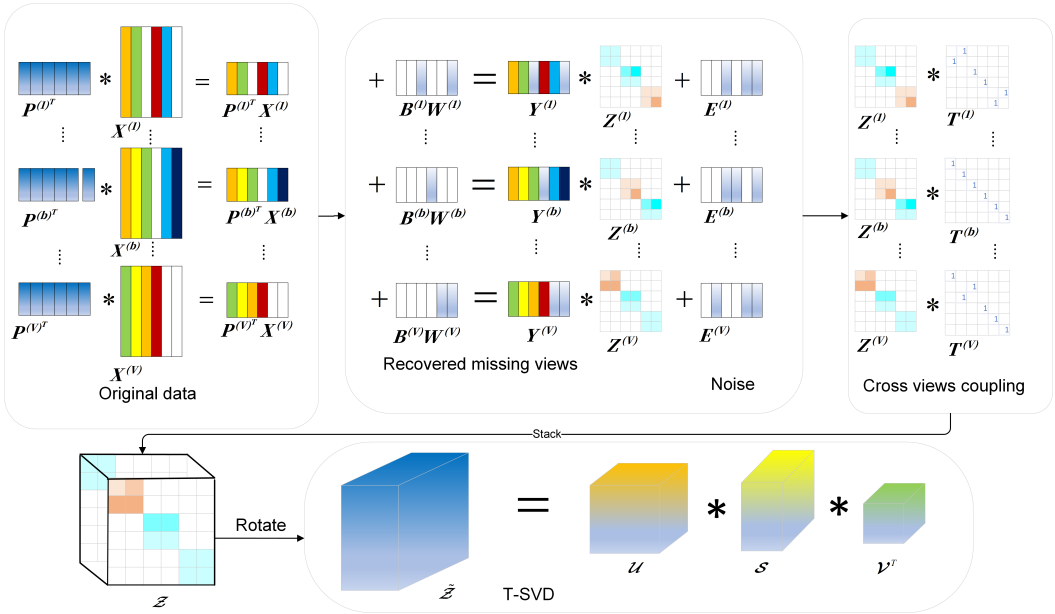

Figure 1. Flowchart of proposed model. First, the incomplete raw data are projected into a low-dimensional space, and missing information is recovered. Self-representation learning is then applied to the recovered data to obtain multi-view similarity matrices. Next, the most reliable view is selected as the template view for cross-view coupled learning. Subsequently, a third-order tensor is constructed using the coupled self-representation matrices, and this tensor is rotated to explore high-order correlations among the view data.

2. Problem Background and Preparations

This section lays the foundation for our proposed method by introducing the fundamental concepts of multi-view data and establishing the notation used throughout the paper. We also define key operations, particularly those related to tensor computations, which play a crucial role in our approach.

2.1. Notation and Descriptions

The main notation used in this paper is summarized in Table 1. Multi-view data represent the same set of samples described by different feature sets, where each feature set is collected from a specific view. Let V denote the total number of available views. The data corresponding to the v-th view ($v = 1, \ldots, V$) are organized into a data matrix, denoted by $\boldsymbol{X}^v \in \mathbb{R}^{d_v \times N}$. Within this matrix, each column represents one of the N samples, and each row corresponds to features specific to the v-th view. Specifically, we write $\boldsymbol{X}^v = [\boldsymbol{x}_1^v, \ldots, \boldsymbol{x}_N^v]$, where $\boldsymbol{x}_k^v \in \mathbb{R}^{d_v \times 1}$ is the k-th sample of the v-th view and d_v is the feature dimension of the v-th view. If the dataset is coupled, it implies that the k-th column vector $\boldsymbol{x}_k^v$ of the v-th view and the k-th column vector $\boldsymbol{x}_k^w$ of the w-th view (for $v \neq w$) correspond to the k-th sample ($k = 1, \ldots, N$).

Table 1. Description of notation.

Notation	Description
$\boldsymbol{A}$	A matrix
$\boldsymbol{\mathcal{A}}$	A tensor
$\|\|\cdot\|\|_F$	Frobenius norm, $\|\|A\|\|_F = \sqrt{\sum_{i,j} a_{ij}^2}$
$\|\|\cdot\|\|_{2,1}$	$l_{2,1}$-norm, $\|\|A\|\|_{2,1} = \sum_j \|\|\boldsymbol{a}(:,j)\|\|_2$
$\|\|\cdot\|\|_*$	Nuclear norm, the sum of singular values
$\|\cdot\|$	Absolute value
V	The number of views
N	The number of samples
k	The number of feature dimensions after dimensionality reduction
n_v	The number of missing samples in the v-th view
d_v	The feature dimension in the v-th view
$\boldsymbol{X}^v \in \mathbb{R}^{d_v \times N}$	The uncoupled data matrix of v-th view
$\boldsymbol{Y}^v \in \mathbb{R}^{d_v \times N}$	The coupled data matrix of v-th view
$\boldsymbol{Z}^v \in \mathbb{R}^{N \times N}$	The view-specifc self-representation matrix of the v-th view
$\boldsymbol{T}^v \in \mathbb{R}^{N \times N}$	The view-specific coupling matrix of the v-th view
$\boldsymbol{E}^b \in \mathbb{R}^{k \times N}$	The error matrix of the v-th view
$\boldsymbol{\mathcal{Z}} \in \mathbb{R}^{N \times N \times V}$	The self-representation tensor
$\boldsymbol{B}^v \in \mathbb{R}^{k \times N_v}$	The filled information of missing samples in the v-th view
$\boldsymbol{W}^v \in \mathbb{R}^{N_v \times N}$	The index matrix of missing samples in the v-th view
$\boldsymbol{P}^v \in \mathbb{R}^{d_v \times k}$	The dimensionality reduction matrix in the v-th view

2.2. Definitions

In this section, we introduce definitions related to tensor nuclear norm operations, which are crucial for exploring high-order correlations across multiple views.

Definition 1 (Block diagonal matrix [10]). *For a third-order tensor $\boldsymbol{\mathcal{A}} \in \mathbb{R}^{n_1 \times n_2 \times n_3}$, its block diagonal matrix is defined as*

$$\mathrm{bdiag}(\boldsymbol{\mathcal{A}}) = \begin{bmatrix} \boldsymbol{A}^1 & & & \\ & \boldsymbol{A}^2 & & \\ & & \ddots & \\ & & & \boldsymbol{A}^{n_3} \end{bmatrix}.$$

Definition 2 (Block circulant matrix [10]). *For a third-order tensor $\boldsymbol{\mathcal{A}} \in \mathbb{R}^{n_1 \times n_2 \times n_3}$, its block circulant matrix is defined as*

$$\mathrm{bcirc}(\boldsymbol{\mathcal{A}}) = \begin{bmatrix} \boldsymbol{A}^1 & \boldsymbol{A}^{n_3} & \cdots & \boldsymbol{A}^2 \\ \boldsymbol{A}^2 & \boldsymbol{A}^1 & \cdots & \boldsymbol{A}^3 \\ \vdots & \vdots & \ddots & \vdots \\ \boldsymbol{A}^{n_3} & \boldsymbol{A}^{n_3-1} & \cdots & \boldsymbol{A}^1 \end{bmatrix}.$$

Definition 3 (Block vectorizing [10]). *For a third-order tensor $\boldsymbol{\mathcal{A}} \in \mathbb{R}^{n_1 \times n_2 \times n_3}$, the block vectorizing and its opposite operation are as follows:*

$$\text{bvec}(\boldsymbol{\mathcal{A}}) = \begin{bmatrix} A^1 \\ A^2 \\ \vdots \\ A^{n_3} \end{bmatrix}, \quad \text{bvfold}(\text{bvec}(\boldsymbol{\mathcal{A}})) = \boldsymbol{\mathcal{A}}.$$

Definition 4 (t-product [10]). *Given two tensors* $\boldsymbol{\mathcal{A}} \in \mathbb{R}^{n_1 \times n_2 \times n_3}$ *and* $\boldsymbol{\mathcal{B}} \in \mathbb{R}^{n_2 \times n_4 \times n_3}$*, the result of the t-product* $\boldsymbol{\mathcal{A}} * \boldsymbol{\mathcal{B}}$ *is a tensor* $\boldsymbol{\mathcal{C}} \in \mathbb{R}^{n_1 \times n_4 \times n_3}$*:*

$$\boldsymbol{\mathcal{C}} = \boldsymbol{\mathcal{A}} * \boldsymbol{\mathcal{B}} = \text{bvfold}(\text{bcirc}(\boldsymbol{\mathcal{A}})\text{bvec}(\boldsymbol{\mathcal{B}})).$$

Definition 5 (f-diagonal tensor [10]). *A tensor is called an f-diagonal tensor if each of its front slices is a diagonal matrix.*

Definition 6 (Identity tensor [10]). *A tensor, represented as* $\boldsymbol{\mathcal{I}}$*, is called an identity tensor if its first front slice is an identity matrix and other front slices are null matrices.*

Definition 7 (Orthogonal tensor [10]). *A tensor is called an orthogonal tensor if it satisfies* $\boldsymbol{\mathcal{A}} * \boldsymbol{\mathcal{A}}^\top = \boldsymbol{\mathcal{I}}$*.*

Definition 8 (Transpose tensor [10]). *Given a tensor* $\mathcal{A} \in \mathbb{R}^{n_1 \times n_2 \times n_3}$*, then the transpose tensor* $\mathcal{A}^\top \in \mathbb{R}^{n_2 \times n_1 \times n_3}$ *is obtained by transposing each front slice and then reversing the order of the transposed frontal slices 2 through* n_3*.*

Definition 9 (t-SVD [10]). *The t-SVD of a tensor* $\boldsymbol{\mathcal{A}} \in \mathbb{R}^{n_1 \times n_2 \times n_3}$ *is defined as follows:*

$$\boldsymbol{\mathcal{A}} = \boldsymbol{\mathcal{U}} * \boldsymbol{\mathcal{S}} * \boldsymbol{\mathcal{V}}^\top,$$

where $\boldsymbol{\mathcal{U}} \in \mathbb{R}^{n_1 \times n_1 \times n_3}$ *and* $\boldsymbol{\mathcal{V}} \in \mathbb{R}^{n_2 \times n_2 \times n_3}$ *are orthogonal tensors and* $\boldsymbol{\mathcal{S}} \in \mathbb{R}^{n_1 \times n_2 \times n_3}$ *is an f-diagonal tensor.*

Definition 10 (Tensor nuclear norm, TNN [10]). *The TNN is defined as the sum of the singular values of each frontal slice of a tensor* $\boldsymbol{\mathcal{A}} \in \mathbb{R}^{n_1 \times n_2 \times n_3}$*, following the given form*

$$\|\boldsymbol{\mathcal{A}}\|_\circledast = \sum_{i=1}^{n_3} \|A^i\|_\circledast = \sum_{i=1}^{n_3} \sum_{j=1}^{l} \sigma_j(A^i),$$

where $l = \min(n_1, n_2)$ *and* σ_j *denotes the j-th largest singular value of* $\boldsymbol{A}^i$*, and* $\boldsymbol{A}^i$ *is i-th frontal slice of* $\boldsymbol{\mathcal{A}}$*.*

2.3. Related Works

In the real world, data are often interfered with by many factors, resulting in some missing data and data uncoupling. In general, the existing IMVC methods can be divided into three categories: subspace-based methods, graph-based methods, and kernel-based methods.

Subspace-based methods assume that the original high-dimensionality data are derived from the low-dimensional subspace. For example, Wang et al. [19] proposed solving the multi-view subspace clustering problem by extending the single-view subspace clustering model to the multi-view subspace domain and enhancing the low-rank property of different views. Zhong et al. [20] integrate similarity graph learning, Laplacian embedding, and discrete indicator matrices into a unified framework. Further, Wang et al. [21] design a deep multi-view subspace clustering method by unifying and discriminant learning. This

can not only discover the local structure of a single view, but also extract the discriminant constraints of all views. Guan et al. [22] utilize graph convolutional networks (GCNs) for multi-view subspace clustering on hyperspectral images.

Graph-based methods construct the similarity graph between samples and learn the uniform affinity matrix. For example, Zheng et al. [23] reconstruct missing samples to mine potential data through potential representation. Han et al. [24] learn self-representation coefficients from multiple views recovered from the sample and decompose each self-representation coefficient into a consistent part and a view-specific part, capturing cross-view similarity and unique information about each view.

Kernel-based methods typically map data from the original low-dimensional space to a high-dimensional feature space. For example, Sinaga et al. [25] proposed an exponential distance-based multi-view fuzzy C-means method, which constructs exponential distances using heat-kernel coefficients. Sinaga et al. [26] further incorporate Gaussian kernel-based exponential distance and a stabilization parameter into the multi-view k-means framework, compressing kernel-weighted distances to reduce sensitivity to outliers and improve clustering robustness.

Although the existing methods have demonstrated promising performance in the field of multi-view clustering, most of them require the original data to be coupled, and their clustering performance declines when dealing with uncoupled data. As far as we know, although there are already some methods [15,16] for handling uncoupled data, they ignore the potential information of the missing samples in some views and cannot make full use of the complementary information among the views.

In order to solve the problem of uncoupled and incomplete multi-view clustering simultaneously, in this paper we propose a new method, TUIMC, which integrates the recovery of missing samples and the coupling of cross-view similarity matrices into a unified framework.

2.3.1. Self-Representation Learning

For multi-view subspace clustering, self-representation learning can excavate low-dimensional structural information embedded in high-dimensional raw data. Given a multi-view dataset $\boldsymbol{X} = [\boldsymbol{X}^1; \ldots; \boldsymbol{X}^V] \in \mathbb{R}^{d \times N}$, where $\boldsymbol{X}^v \in \mathbb{R}^{d_v \times N}$, $d = \sum_{v=1}^{V} d_v$, d_v is the feature dimension of the original feature space in the v-th view, and N is the number of samples, the general representation model of the multi-view subspace clustering method is as follows:

$$\begin{aligned} &\min_{\boldsymbol{Z}^v, \boldsymbol{E}^v} \sum_{v=1}^{V} (\Omega(\boldsymbol{Z}^v) + \lambda \Theta(\boldsymbol{E}^v)) \\ &s.t.\ \boldsymbol{Y}^v = \boldsymbol{Y}^v \boldsymbol{Z}^v + \boldsymbol{E}^v, \end{aligned} \tag{1}$$

where $\Omega(\cdot)$ and $\Theta(\cdot)$ are functions used to constrain the similarity matrices and noise matrices, λ is a tradeoff parameter, $\boldsymbol{Z}^v \in \mathbb{R}^{N \times N}$ is the coupled similarity matrix of the v-th view, $\boldsymbol{Y}^v \in \mathbb{R}^{d_v \times N}$ is the coupled data matrix, and $\boldsymbol{E}^v \in \mathbb{R}^{d_v \times N}$ is the noise matrix of the v-th view.

However, when the original data are uncoupled, the relationship between the self-representation matrices across views is unknown. Obviously, $\boldsymbol{Z}^v$ cannot be used for efficient clustering in the previous methods [27]. Therefore, these models cannot efficiently solve the clustering problem of uncoupled multi-view data.

2.3.2. Missing Sample Recovery

In real-world scenarios, samples that are missing in some views are not available. However, model (1) assumes that multi-view data are complete; we use the index matrix

$\boldsymbol{W^v} \in \mathbb{R}^{n_v \times N}$ to record the index information of the missing samples in the v-th view. This is defined as follows:

$$\boldsymbol{W}_{i,j}^{v} = \begin{cases} 1 & \text{if } i\text{-th missing instance is } j\text{-th} \\ & \text{instance in } v\text{-th view;} \\ 0 & \text{otherwise.} \end{cases} \tag{2}$$

The missing samples can be recovered by the filling matrix $\boldsymbol{B^v}$ [24]. Therefore, considering the missing multi-view data, model (1) can be rewritten as follows:

$$\begin{aligned} &\min_{\boldsymbol{Z}^v, \boldsymbol{E}^v} \sum_{v=1}^{V} (\Omega(\boldsymbol{Z}^v) + \lambda \Theta(\boldsymbol{E}^v)) \\ &s.t.\ \boldsymbol{X}^v + \boldsymbol{B}^v \boldsymbol{W}^v = (\boldsymbol{X}^v + \boldsymbol{B}^v \boldsymbol{W}^v)\boldsymbol{Z}^v + \boldsymbol{E}^v, \end{aligned} \tag{3}$$

where $\boldsymbol{X}^v$ is the original incomplete data matrix of the v-th view, and the missing samples are represented by zeros. $\boldsymbol{B}^v\boldsymbol{W}^v$ is used to recover the missing samples in the original multi-view data.

3. Methodology

In this section, we elaborate in detail on the proposed Tensor-based Uncoupled and Incomplete Multi-view Clustering (TUIMC) model. To better understand the design rationale and individual components of the model, we first need to clarify the problem it aims to solve and the key motivations behind it. Below, we specifically discuss each module, as each directly shapes the concrete architecture of the TUIMC model.

3.1. Primary Motivations

A significant challenge encountered in practical applications of multi-view data is the issue of uncoupled views. This occurs when samples do not directly correspond across the different feature representations, making the effective fusion of information from these diverse perspectives for clustering tasks particularly critical. Therefore, developing a mechanism to establish or enforce inter-view relationships, thereby enabling effective cross-view learning, constitutes a primary problem that our model must address.

In model (3), the original data are restored, but the information in the original high-dimensional space is redundant. Therefore, it is necessary to consider the key information of the samples while recovering the original data.

The following section details the specific cross-view coupling strategy and low-dimensional sample recovery we employ to tackle these issues.

3.1.1. Cross-View Coupling

In some practical applications, data from different views may be acquired under different time, environmental, or conditional contexts. For example, the image of an object and its corresponding textual description may not be generated simultaneously, leading to temporal delays or differences in the contexts of data collection. Such sampling inconsistencies can cause alignment issues between views. To efficiently address this alignment issue, we first designate one view as the template view, and then apply a coupling matrix $\boldsymbol{T}^v$ to perform column transformations on the other similarity matrices according to the template view. This coupling can be denoted as follows:

$$\begin{aligned} &\min_{\boldsymbol{Z}^v,\boldsymbol{T}^v} \sum_{v=1}^{V} ||\boldsymbol{Z}^b - \boldsymbol{Z}^v\boldsymbol{T}^v||_F^2. \\ &s.t. \boldsymbol{T}^v \in \{0,1\}, \boldsymbol{T}^v\mathbf{1} = 1, {\boldsymbol{T}^v}^\top\mathbf{1} = 1. \end{aligned} \tag{4}$$

The above model (4) increases the cross-view correspondence between the self-representation matrix $\boldsymbol{Z}^v$ obtained from the reconstructed subspace data, and couples the self-representation matrix of other views with the self-representation matrix of the most reliable view. A schematic diagram of the alignment of self-representation matrices is shown in Figure 2.

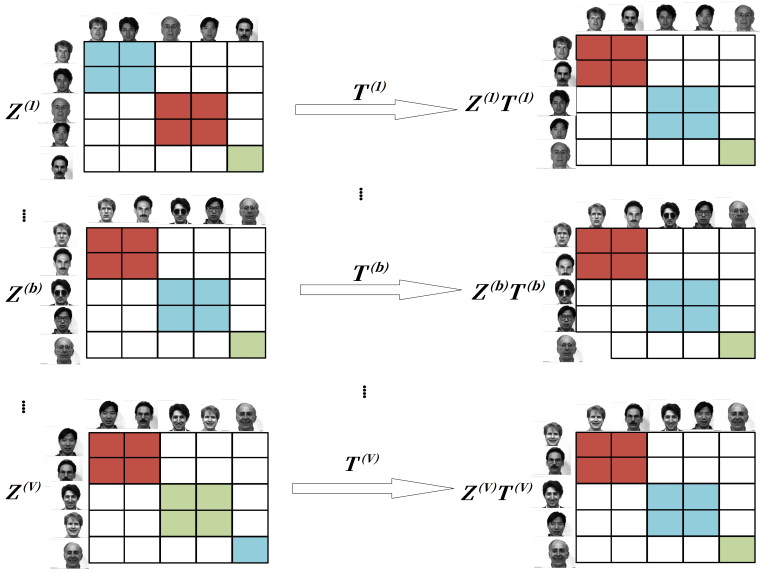

Figure 2. The similarity matrix $\boldsymbol{Z}^v$ is aligned with the template view b through column-wise transformation using a permutation matrix $\boldsymbol{T}^v$.

Lemma 1 ([28]). *For any vectors* $\boldsymbol{a}$ *and* $\boldsymbol{b}$, *let* $\tilde{\boldsymbol{a}} = \boldsymbol{H}\boldsymbol{a}$ *and* $\tilde{\boldsymbol{b}} = \boldsymbol{H}\boldsymbol{b}$, *where* $\boldsymbol{H}\boldsymbol{H}^\top = \boldsymbol{H}^\top\boldsymbol{H} = \boldsymbol{I}$. *Then,* $\|\tilde{\boldsymbol{a}}\|_2 = \|\boldsymbol{a}\|_2$, $\|\tilde{\boldsymbol{b}}\|_2 = \|\boldsymbol{b}\|_2$, $\bar{\boldsymbol{a}} \cdot \bar{\boldsymbol{b}} = \boldsymbol{a} \cdot \boldsymbol{b}$, *which implies* $\cos(\bar{\boldsymbol{a}}, \bar{\boldsymbol{b}}) = \cos(\boldsymbol{a}, \boldsymbol{b})$ *and* $\|\bar{\boldsymbol{a}} - \bar{\boldsymbol{b}}\|_2 = \|\boldsymbol{a} - \boldsymbol{b}\|_2$.

The optimal solution of model (4) with regard to $\boldsymbol{T}^v$ is discrete and difficult to solve. Therefore, according to Lemma 1, we relax these constraints $\boldsymbol{T}^v \in \{0,1\}$, $\boldsymbol{T}^v\mathbf{1} = 1$, ${\boldsymbol{T}^v}^\top\mathbf{1} = 1$ in model (4) to $\boldsymbol{T}^v{\boldsymbol{T}^v}^\top = \boldsymbol{I}$.

3.1.2. Joint Low-Dimensional Subspace Learning and Sample Recovery

In the original high-dimensional space, the complexity of the dimensions may lead to issues such as overfitting when recovering missing data. In contrast, low-dimensional spaces are typically able to retain the core information of the data while mitigating the interference caused by redundant data in high-dimensional spaces. Therefore, conducting missing data recovery and subspace learning in a low-dimensional space can better preserve the relative relationships among samples, resulting in more accurate and consistent clustering performance. This joint low-dimensional subspace learning and sample recovery can be denoted as follows:

$$\begin{aligned} &\min_{\boldsymbol{Z}^v,\boldsymbol{E}^v,\boldsymbol{P}^v} \sum_{v=1}^{V} (\Omega(\boldsymbol{Z}^v) + \lambda\Theta(\boldsymbol{E}^v)) \\ &s.t. \quad {\boldsymbol{P}^v}^\top\boldsymbol{X}^v + \boldsymbol{B}^v\boldsymbol{W}^v = ({\boldsymbol{P}^v}^\top\boldsymbol{X}^v + \boldsymbol{B}^v\boldsymbol{W}^v)\boldsymbol{Z}^v + \boldsymbol{E}^v, \\ &\quad\; \boldsymbol{P}^v{\boldsymbol{P}^v}^\top = \boldsymbol{I}, \end{aligned} \tag{5}$$

where $\boldsymbol{P}^v \in \mathbb{R}^{d_v \times k}$ is the projection matrix used to project the high-dimensional matrix into a k-dimensional space ($k \ll d_v$); $\boldsymbol{P}^v \boldsymbol{P}^{v^\top} = \boldsymbol{I}$ enhances the diversity of the projected low-dimensional features.

3.2. The Proposed Model

Taking into account all the above considerations, the proposed model is ultimately denoted as follows:

$$\begin{aligned} &\min_{\boldsymbol{Z}^v, \boldsymbol{T}^v, \alpha^v, \boldsymbol{E}^v, \boldsymbol{P}^v, \boldsymbol{B}^v} \lambda_1 ||\boldsymbol{\mathcal{Z}}||_{\circledast} + \sum_{v=1}^{V} \alpha_v^r ||\boldsymbol{Z}^b - \boldsymbol{Z}^v \boldsymbol{T}^v||_F^2 + \lambda_2 \sum_{v=1}^{V} ||\boldsymbol{E}^v||_{2,1} \\ &s.t. \quad \boldsymbol{P}^{v^\top} \boldsymbol{X}^v + \boldsymbol{B}^v \boldsymbol{W}^v = (\boldsymbol{P}^{v^\top} \boldsymbol{X}^v + \boldsymbol{B}^v \boldsymbol{W}^v) \boldsymbol{Z}^v + \boldsymbol{E}^v, \\ &\boldsymbol{\mathcal{Z}} = \Psi(\boldsymbol{Z}^1 \boldsymbol{T}^1, \boldsymbol{Z}^2 \boldsymbol{T}^2, \ldots, \boldsymbol{Z}^V \boldsymbol{T}^V), \\ &\boldsymbol{P}^v \boldsymbol{P}^{v^\top} = \boldsymbol{I}, \boldsymbol{T}^v \boldsymbol{T}^{v^\top} = \boldsymbol{I}, \end{aligned} \tag{6}$$

where $||\cdot||_{\circledast}$ denotes the tensor nuclear norm, $||\cdot||_{2,1}$ denotes the $l_{2,1}$-norm, $\Psi()$ denotes the operation of stacking all matrices into a third-order tensor, λ_1 and λ_2 are tradeoff parameters, and α_v is an adaptive parameter of the v-th view.

3.3. Optimization

Solving the problem (38) directly is very difficult because it involves multiple variables. Therefore, we solve the problem using the alternating direction method of multipliers [18] by introducing auxiliary variables $\boldsymbol{M}^v$ and $\boldsymbol{\mathcal{K}}$. Let $\boldsymbol{M}^v = \boldsymbol{T}^v$ and $\boldsymbol{\mathcal{K}} = \boldsymbol{\mathcal{Z}}$. The Lagrange function of problem (38) is denoted as follows:

$$\begin{aligned} &\min_{\varphi} \lambda_1 ||\boldsymbol{\mathcal{K}}||_{\circledast} + \sum_{v=1}^{V} \alpha_v^r ||\boldsymbol{Z}^b - \boldsymbol{Z}^v \boldsymbol{M}^v||_F^2 + \lambda_2 ||\boldsymbol{E}||_{2,1} \\ &+ \frac{\mu}{2} ||\boldsymbol{P}^{v^\top} \boldsymbol{X}^v + \boldsymbol{B}^v \boldsymbol{W}^v - (\boldsymbol{P}^{v^\top} \boldsymbol{X}^v + \boldsymbol{B}^v \boldsymbol{W}^v) \boldsymbol{Z}^v - \boldsymbol{E}^v||_F^2 \\ &+ \langle \boldsymbol{J}^v, \boldsymbol{P}^{v^\top} \boldsymbol{X}^v + \boldsymbol{B}^v \boldsymbol{W}^v - (\boldsymbol{P}^{v^\top} \boldsymbol{X}^v + \boldsymbol{B}^v \boldsymbol{W}^v) \boldsymbol{Z}^v - \boldsymbol{E}^v \rangle \\ &+ \langle \boldsymbol{G}^v, \boldsymbol{T}^v - \boldsymbol{M}^v \rangle + \frac{\mu}{2} ||\boldsymbol{T}^v - \boldsymbol{M}^v||_F^2 + \langle \boldsymbol{\mathcal{Y}}, \boldsymbol{\mathcal{Z}} - \boldsymbol{\mathcal{K}} \rangle \\ &+ \frac{\mu}{2} ||\boldsymbol{\mathcal{Z}} - \boldsymbol{\mathcal{K}}||_F^2, \end{aligned} \tag{7}$$

where $\varphi = \{\boldsymbol{Z}^v, \boldsymbol{T}^v, \alpha^v, \boldsymbol{M}^v, \boldsymbol{E}^v, \boldsymbol{P}^v, \boldsymbol{B}^v, \boldsymbol{J}^v, \boldsymbol{G}^v, \boldsymbol{\mathcal{K}}, \boldsymbol{\mathcal{Y}}\}$. $\boldsymbol{J}^v$, $\boldsymbol{G}^v$, and $\boldsymbol{\mathcal{Y}}$ are Lagrangian multipliers, and μ is a penalty parameter.

Update $\boldsymbol{Z}^{(v)}$: For the v-th view, with all variables except $\boldsymbol{Z}^{(v)}$ fixed, problem (7) can be expressed as follows:

$$\begin{aligned} &\min_{\boldsymbol{Z}^v} \alpha_v^r ||\boldsymbol{Z}^b - \boldsymbol{Z}^v \boldsymbol{M}^v||_F^2 + \frac{\mu}{2} ||\boldsymbol{Z}^v \boldsymbol{T}^v - \boldsymbol{K}^v + \frac{\boldsymbol{Y}^v}{\mu}||_F^2 \\ &+ \frac{\mu}{2} ||\boldsymbol{P}^{v^\top} \boldsymbol{X}^v + \boldsymbol{B}^v \boldsymbol{W}^v - (\boldsymbol{P}^{v^\top} \boldsymbol{X}^v + \boldsymbol{B}^v \boldsymbol{W}^v) \boldsymbol{Z}^v - \boldsymbol{E}^v + \frac{\boldsymbol{J}^v}{\mu}||_F^2. \end{aligned} \tag{8}$$

By setting the derivative of (8) with respect to $\boldsymbol{Z}^v$ to zero, the result of $\boldsymbol{Z}^{v^*}$ can be obtained by

$$\begin{aligned} \boldsymbol{Z}^{v^*} &= [\mu \boldsymbol{D}^{v^\top} \boldsymbol{D}^v + (2\alpha_v^r + \mu) \boldsymbol{I}]^{-1} [2\alpha_v^r \boldsymbol{Z}^b \boldsymbol{M}^{v^\top} + \mu \boldsymbol{K}^v \boldsymbol{T}^{v^\top} \\ &- \boldsymbol{Y}^v \boldsymbol{Y}^{v^\top} + \mu \boldsymbol{D}^{v^\top} (\boldsymbol{D}^v - \boldsymbol{E}^v + \frac{\boldsymbol{J}^v}{\mu})], \end{aligned} \tag{9}$$

where $\boldsymbol{D}^v = \boldsymbol{P}^{v^\top} \boldsymbol{X}^v + \boldsymbol{B}^v \boldsymbol{W}^v$.

Update $\boldsymbol{M}^v$: By fixing all the variables expect $\boldsymbol{M}^v$, problem (7) can be written as

$$\begin{aligned} &\min_{\boldsymbol{M}^v} \alpha^v ||\boldsymbol{Z}^b - \boldsymbol{Z}^v \boldsymbol{M}^v||_F^2 + \frac{\mu}{2} ||\boldsymbol{T}^v - \boldsymbol{M}^v + \frac{\boldsymbol{G}^v}{\mu}||_F^2 \\ &s.t. \quad \boldsymbol{M}^v \boldsymbol{M}^{v^\top} = \boldsymbol{I}. \end{aligned} \tag{10}$$

Problem (10) can be rewritten as

$$\begin{aligned} &\max_{\boldsymbol{M}^v} Tr[\boldsymbol{M}^{v^\top} (2\alpha_v^r \boldsymbol{Z}^{v^\top} \boldsymbol{Z}^v + \mu \boldsymbol{T}^v - \boldsymbol{G}^v)] \\ &s.t. \quad \boldsymbol{M}^v \boldsymbol{M}^{v^\top} = \boldsymbol{I}, \end{aligned} \tag{11}$$

where $\boldsymbol{Q}^v = 2\alpha_v^r \boldsymbol{Z}^{v^\top} \boldsymbol{Z}^v + \mu \boldsymbol{T}^v - \boldsymbol{G}^v$. According to [29], we can obtain the optimal solution of $\boldsymbol{M}^v$ as follows:

$$\boldsymbol{M}^{v^*} = \boldsymbol{U}_m \boldsymbol{V}_m^\top, \tag{12}$$

where $\boldsymbol{U}_m$ and $\boldsymbol{V}_m$ represent the matrices which comprise the first left singular vectors and right singular vectors of $\boldsymbol{Q}^v$.

Update $\boldsymbol{T}^v$: By fixing all the variables expect $\boldsymbol{T}^v$, problem (7) can be written as

$$\begin{aligned} &\min_{\boldsymbol{T}^v} \frac{\mu}{2} ||\boldsymbol{T}^v - \boldsymbol{M}^v + \frac{\boldsymbol{G}^v}{\mu}||_F^2 + \frac{\mu}{2} ||\boldsymbol{Z}^v \boldsymbol{T}^v - \boldsymbol{K}^v + \frac{\boldsymbol{Y}^v}{\mu}||_F^2 \\ &s.t. \quad \boldsymbol{T}^v \boldsymbol{T}^{v^\top} = \boldsymbol{I}. \end{aligned} \tag{13}$$

Problem (13) can be rewritten as

$$\begin{aligned} &\max_{\boldsymbol{T}^v} Tr[\boldsymbol{T}^{v^\top} (\boldsymbol{M}^v - \frac{\boldsymbol{G}^v}{\mu} - \frac{\boldsymbol{Z}^{v^\top} \boldsymbol{Y}^v}{\mu})] \\ &s.t. \quad \boldsymbol{T}^v \boldsymbol{T}^{v^\top} = \boldsymbol{I}. \end{aligned} \tag{14}$$

where $\boldsymbol{Q}^v$ as $(\boldsymbol{M}^v - \frac{\boldsymbol{G}^v}{\mu} - \frac{\boldsymbol{Z}^{v^\top} \boldsymbol{Y}^v}{\mu})$. Similar to the method used to update $\boldsymbol{M}^v$, we can obtain the updated $\boldsymbol{T}^v$ as follows:

$$\boldsymbol{T}^{v^*} = \boldsymbol{U}_m \boldsymbol{V}_m^T, \tag{15}$$

where $\boldsymbol{U}_m$ and $\boldsymbol{V}_m$ represent the matrices which comprise the first left singular vectors and right singular vectors of $\boldsymbol{Q}^v$.

Lemma 2 ([30]). *For a matrix $\boldsymbol{U}$, for the following optimization problem,*

$$\min_{\boldsymbol{E}} \lambda ||\boldsymbol{E}||_{2,1} + \frac{1}{2} ||\boldsymbol{E} - \boldsymbol{U}||_F^2, \tag{16}$$

let $\boldsymbol{E}^*$ be the optimal solution; the i-th column of $\boldsymbol{E}^*$ is

$$[\boldsymbol{E}^*]_{:,i} = \begin{cases} \frac{||\boldsymbol{U}_{:,i}||_2 - \lambda}{||\boldsymbol{U}_{:,i}||_2} \boldsymbol{U}_{:,i}, & \text{if } ||\boldsymbol{U}_{:,i}||_2 > \lambda; \\ 0, & \text{otherwise.} \end{cases} \tag{17}$$

Update $\boldsymbol{E}^v$: By fixing all the variables expect $\boldsymbol{E}^v$, the problem in (7) can be written as

$$\begin{aligned} &\min_{\boldsymbol{E}^v} \frac{\lambda_2}{\mu} ||\boldsymbol{E}^v||_{2,1}^2 + \frac{1}{2} |\boldsymbol{P}^{v^\top} \boldsymbol{X}^v + \boldsymbol{B}^v \boldsymbol{W}^v - (\boldsymbol{P}^{v^\top} \boldsymbol{X}^v + \boldsymbol{B}^v \boldsymbol{W}^v) \boldsymbol{Z}^v \\ &- \boldsymbol{E}^v||_F^2. \end{aligned} \tag{18}$$

Problem (18) can be rewritten as

$$\min_{\boldsymbol{E}^v} \frac{\lambda_2}{\mu}||\boldsymbol{E}^v||_{2,1}^2 + \frac{1}{2}||\boldsymbol{A}^v - \boldsymbol{E}^v||_F^2, \tag{19}$$

where $\boldsymbol{A}^v = \boldsymbol{P}^{v^\top}\boldsymbol{X}^v + \boldsymbol{B}^v\boldsymbol{W}^v - (\boldsymbol{P}^{v^\top}\boldsymbol{X}^v + \boldsymbol{B}^v\boldsymbol{W}^v)\boldsymbol{Z}^v + \frac{\boldsymbol{J}^v}{\mu}$. According to Lemma 2, we have the following solution:

$$\boldsymbol{E}^*_{:,i} = \begin{cases} \dfrac{\|\boldsymbol{A}_{:,i}\|_2 - \dfrac{\lambda_2}{\mu}}{\|\boldsymbol{A}_{:,i}\|_2} & \text{if } \|\boldsymbol{A}_{:,i}\|_2 > \dfrac{\lambda_2}{\mu}; \\ 0 & \text{otherwise.} \end{cases} \tag{20}$$

Update $\boldsymbol{P}^v$: By fixing all the variables expect $\boldsymbol{P}^v$, problem (7) can be written as

$$\begin{aligned} &\min_{\boldsymbol{P}^v} ||\boldsymbol{P}^{v^\top}\boldsymbol{X}^v + \boldsymbol{B}^v\boldsymbol{W}^v - (\boldsymbol{P}^{v^\top}\boldsymbol{X}^v + \boldsymbol{B}^v\boldsymbol{W}^v)\boldsymbol{Z}^v - \boldsymbol{E}^v + \frac{\boldsymbol{J}^v}{\mu}||_F^2 \\ &s.t. \quad \boldsymbol{P}^v\boldsymbol{P}^{v^\top} = \boldsymbol{I}. \end{aligned} \tag{21}$$

Problem (21) can be rewritten as follows:

$$\begin{aligned} &\max_{\boldsymbol{P}^v} Tr[\boldsymbol{P}^{v^\top}(\boldsymbol{X}^v\boldsymbol{Z}^v - \boldsymbol{X}^v)(\boldsymbol{B}^v\boldsymbol{W}^v - \boldsymbol{B}^v\boldsymbol{W}^v\boldsymbol{Z}^v - \boldsymbol{E}^v + \frac{\boldsymbol{J}^v}{\mu})^T]. \\ &s.t. \quad \boldsymbol{P}^v\boldsymbol{P}^{v^\top} = \boldsymbol{I}. \end{aligned} \tag{22}$$

Let $\boldsymbol{Q}^v = (\boldsymbol{X}^v\boldsymbol{Z}^v - \boldsymbol{X}^v)(\boldsymbol{B}^v\boldsymbol{W}^v - \boldsymbol{B}^v\boldsymbol{W}^v\boldsymbol{Z}^v - \boldsymbol{E}^v + \frac{\boldsymbol{J}^v}{\mu})^T$.

Similar to $\boldsymbol{T}^v$, we can obtain

$$\boldsymbol{P}^{v^*} = \boldsymbol{U}_m\boldsymbol{V}_m^T, \tag{23}$$

where $\boldsymbol{U}_m$ and $\boldsymbol{V}_m$ represent the matrices which comprise the first m left singular vectors and right singular vectors of $\boldsymbol{Q}^v$.

Update $\boldsymbol{B}^v$: By fixing all the variables expect $\boldsymbol{B}^v$, problem (7) can be written as

$$\min_{\boldsymbol{B}^v} ||\boldsymbol{P}^{v^\top}\boldsymbol{X}^v + \boldsymbol{B}^v\boldsymbol{W}^v - (\boldsymbol{P}^{v^\top}\boldsymbol{X}^v + \boldsymbol{B}^v\boldsymbol{W}^v)\boldsymbol{Z}^v - \boldsymbol{E}^v + \frac{\boldsymbol{J}^v}{\mu}||_F^2. \tag{24}$$

The optimal solution $\boldsymbol{B}^{v^*}$ can be obtained by differentiating problem (24) with respect to $\boldsymbol{B}^v$ and setting it to zero as follows.

$$\boldsymbol{B}^{v^*} = (\boldsymbol{P}^{v^\top}\boldsymbol{X}^v\boldsymbol{Z}^v - \boldsymbol{P}^{v^\top}\boldsymbol{X}^v + \boldsymbol{E}^v - \frac{\boldsymbol{J}^v}{\mu})\boldsymbol{A}^\top(\boldsymbol{A}\boldsymbol{A}^\top)^{-1}, \tag{25}$$

where $\boldsymbol{A}^v = (\boldsymbol{W}^v - \boldsymbol{W}^v\boldsymbol{Z}^v)$.

Update α_v: By fixing all the variables expect α_v, problem (7) can be written as

$$\begin{aligned} &\min_{\alpha_v} \sum_{v=1}^{V} \alpha_v^r ||\boldsymbol{Z}^b - \boldsymbol{Z}^v\boldsymbol{M}^v||_F^2 \\ &s.t. \quad 0 \le \alpha_v \le 1, \quad \sum_{v=1}^{V} \alpha_v = 1. \end{aligned} \tag{26}$$

Let $q_v = ||\boldsymbol{Z}^b - \boldsymbol{Z}^v\boldsymbol{M}^v||_F^2$; the Lagrange function of the problem (26) is as follows:

$$\min_{\alpha_v,\mu} \sum_{v=1}^{V} \alpha_v q_v - \mu\Big(\sum_{v=1}^{V} \alpha_v - 1\Big). \tag{27}$$

Setting the derivative of problem (27) with respect to α_v to zero, we can obtain

$$\alpha_v = \frac{\mu^{\frac{1}{r-1}}}{(rq_v)^{\frac{1}{r-1}}}. \tag{28}$$

According to the constraints $\sum_{v=1}^{V} \alpha_v = 1$, we can further derive the optimal solution of α_v as follows:

$$\alpha_v = \frac{q_v^{\frac{1}{r-1}}}{\sum_{v=1}^{V} q_v^{\frac{1}{r-1}}}. \tag{29}$$

Update $\mathcal{K}$: By fixing all the variables expect $\mathcal{K}$, problem (7) can be written as

$$\min_{\mathcal{K}} \frac{\lambda_1}{\mu}||\mathcal{K}||_{\circledast} + \frac{1}{2}||\mathcal{Z} - \mathcal{K} + \frac{\mathcal{Y}}{\mu}||_F^2. \tag{30}$$

This problem is a typical t-SVD-based tensor nuclear norm minimization problem, and has the following approximate solutions:

$$\mathcal{K}^* = \mathcal{U} * \boldsymbol{\varphi}_{\boldsymbol{m/u}}(\mathcal{S}) * \mathcal{V}^\top. \tag{31}$$

where $\mathcal{Z} + \frac{\mathcal{Y}}{\mu} = \mathcal{U} * \mathcal{S} * \mathcal{V}^\top$ is obtained by the t-SVD operation. $\varphi_{V/\mu}(\mathcal{S}) = \mathcal{S} * \mathcal{F}$, $\mathcal{F} \in \mathbb{R}^{N\times N\times V}$ is an f-diagonal tensor whose diagonal elements in the Fourier domain are expressed as

$$\hat{\mathcal{F}}(i,i,j) = \max\left\{1 - \frac{V/\mu}{\hat{\mathcal{S}}(i,i,j)}, 0\right\}. \tag{32}$$

The Lagrange multipliers can be updated as follows:

$$\boldsymbol{J}^{v^*} = \boldsymbol{J}^v + \mu\Big[\boldsymbol{P}^{v^\top}\boldsymbol{X}^v + \boldsymbol{B}^v\boldsymbol{W}^v - (\boldsymbol{P}^{v^\top}\boldsymbol{X}^v + \boldsymbol{B}^v\boldsymbol{W}^v)\boldsymbol{Z}^v - \boldsymbol{E}^v\Big], \tag{33}$$

$$\boldsymbol{G}^{v^*} = \boldsymbol{G}^v + \mu(\boldsymbol{T}^v - \boldsymbol{M}^v), \tag{34}$$

$$\mathcal{Y}^* = \mathcal{Y} + \mu(\mathcal{Z} - \mathcal{K}). \tag{35}$$

The penalty parameter μ is updated as follows:

$$\mu^* = \min(\eta\mu, \mu_{max}). \tag{36}$$

where η is a constant greater than 1 used to expedite convergence, and μ_{max} is the maximum value of the penalty parameter μ.

The convergence conditions are set as follows:

$$\left\{\begin{array}{c} \sum_{v=1}^{V} \frac{1}{V}||\boldsymbol{P}^{v^\top}\boldsymbol{X}^v + \boldsymbol{B}^v\boldsymbol{W}^v - \Big(\boldsymbol{P}^{v^\top}\boldsymbol{X}^v + \boldsymbol{B}^v\boldsymbol{W}^v\Big)\boldsymbol{Z}^v - \boldsymbol{E}^v||_\infty \\ \sum_{v=1}^{V} \frac{1}{V}||\boldsymbol{T}^v - \boldsymbol{M}^v||_\infty \end{array}\right\} < \varepsilon, \tag{37}$$

where ε is the convergence threshold. Algorithm 1 outlines the procedure for solving the problem (7).

Algorithm 1 TUIMC for multi-view clustering.

Input: Incomplete multi-view data: $\{\boldsymbol{X}^1, \ldots, \boldsymbol{X}^V\}$, the index matrices $\{\boldsymbol{W}^1, \ldots, \boldsymbol{W}^V\}$, λ_1, λ_2, dimensionality reduction k, and the index b of the template view.
Initialize: $\boldsymbol{T}^v = \boldsymbol{I}$, $\boldsymbol{M}^v = \boldsymbol{J}^v = \boldsymbol{G}^v = \boldsymbol{Y}^v = \boldsymbol{P}^v = \boldsymbol{B}^v = \boldsymbol{0}$, $\mathcal{K} = \boldsymbol{0}$, $\alpha_v = 1/V$, $r = 2$, $\mu = 10^{-5}$, $\mu_{max} = 10^{10}$, $Iter_{max} = 100$, $\varepsilon = 10^{-5}$.
while not convergence **do**
1. Update $\boldsymbol{P}^v$ by Equation (23);
2. Update $\boldsymbol{B}^v$ by Equation (25);
3. Update $\boldsymbol{Z}^v$ by Equation (9);
4. Update $\boldsymbol{M}^v$ by Equation (12);
5. Update $\boldsymbol{T}^v$ by Equation (15);
6. Update $\boldsymbol{E}^v$ by Equation (20);
7. Update $\boldsymbol{J}^v$ by Equation (33);
8. Update $\boldsymbol{G}^v$ by Equation (34);
9. Update $\boldsymbol{\alpha}_v$ by Equation (29);
10. Update $\mathcal{Z} = \Psi(\boldsymbol{Z}^1\boldsymbol{P}^1, \ldots, \boldsymbol{Z}^V\boldsymbol{P}^V)$;
11. Update $\mathcal{K}$ by Equation (31);
12. Update $\mathcal{Y}$ by Equation (35);
13. Update parameter μ by Equation (36);
14. Check the convergence condition (37);
15. **until** Convergence
16. Obtain the clustering results using the spectral clustering method on the affinity matrix $\frac{1}{V}\sum_{v=1}^{V}\left(|\boldsymbol{Z}^v\boldsymbol{T}^v| + |\boldsymbol{T}^{v^\top}\boldsymbol{Z}^{v^\top}|\right)$.

end

3.4. Complexity Analysis

The computational complexity of Algorithm 1 is listed in Table 2, where S represents the number of iterations.

Table 2. The computational cost of Algorithm 1, where d represents the maximum number of multi-view features.

Subproblem	Step	Complexity
$\boldsymbol{B}^v$	Equation (25)	$O(VN^3)$
$\boldsymbol{P}^v$	Equation (23)	$O(VN^3)$
$\boldsymbol{Z}^v$	Equation (9)	$O(VN^3)$
$\boldsymbol{M}^v$	Equation (12)	$O(VN^3)$
$\boldsymbol{T}^v$	Equation (15)	$O(VN^3)$
$\boldsymbol{E}^v$	Equation (20)	$O(VN^2)$
$\mathcal{K}$	Equation (31)	$O(N^2Vlog(N))$
α_v	Equation (29)	$O(VN^2)$
Total		$O(SV(N^2log(N) + N^3))$

4. Experimental Results and Analysis

The following experiments are specifically designed to evaluate how our proposed TUIMC method performs in addressing the fundamental issue, particularly when simultaneously confronted with the additional challenge of incomplete data.

4.1. Multi-View Datasets

The experiments utilized five real-world datasets, including **Yale** and **YaleA** (https://cvc.yale.edu/projects/yalefaces/yalefaces.html), **BBCSport** (http://mlg.ucd.ie/datasets/segment.html), **COIL20** (https://cave.cs.columbia.edu/repository/COIL-20), and **ORL**

(https://www.cl.cam.ac.uk/research/dtg/attarchive/facedatabase.html). The specific details are shown in Table 3. During the experiments, we first shuffle each view to generate uncoupled data, and then perform missing-data processing to obtain the datasets used for the experiments.

Table 3. Summary of different datasets.

Dataset	Yale	YaleA	ORL	BBCSport	COIL20
Content	Face	Face	Face	News	Objects
Clusters	15	15	40	5	20
Samples	165	165	400	169	1440
View1	Intensity (4096)	Color Moment (9)	Intensity (4096)	V1 (3183)	V1 (1024)
View2	LBP (3304)	LBP (50)	Reuters (3631)	V2 (3203)	V2 (6750)
View3	V3 (6750)	GIST (512)	Gabor (6750)	-	V3 (3304)

4.2. Incomplete Data Construction

In the real world, imbalanced and incomplete multi-view data characterized by view-specific missing rates are more common, which poses significant challenges to the clustering process. The missing rates vary between different views, which may lead to information asymmetry. Therefore, we set the average missing rate vector m according to reference [31], and introduce different degrees of incompleteness for different views. The missing rates we set for the different datasets are shown in Table 4. For instance, in the COIL20 dataset, if $m = 0.5$, the missing rate for view 1 is $1.80 \times 0.5 = 0.9$, view 2 is $1.00 \times 0.5 = 0.5$, and view 3 is $0.2 \times 0.5 = 0.1$.

Table 4. Missing rate for each view on different datasets.

Dataset	BBCSport	Yale	YaleA	COIL20	ORL
View1	$0.20 \times m$	$1.80 \times m$	$1.80 \times m$	$1.80 \times m$	$1.80 \times m$
View2	$1.00 \times m$	$1.00 \times m$	$1.00 \times m$	$1.00 \times m$	$1.00 \times m$
View3	–	$0.20 \times m$	$0.20 \times m$	$0.20 \times m$	$0.20 \times m$

4.3. Comparative Models

In our experiments, we employ nine multi-view clustering methods spanning diverse methodologies, including graph-based, subspace learning-based, anchor-based, and uncoupled approaches. The specific methods are detailed as follows:

Graph-based methods: **HCLS-CGL** (https://github.com/ckghostwj/CVPR2023_code/tree/main/HCLS_CGL_code) [32] combines consensus graph learning, confidence graph constraint, and local structure constraint. **UEAF** (https://github.com/ckghostwj/Unified-Embedding-Alignment-with-Missing-Views-Inferring-for-Incomplete-Multi-View-Clustering) [33] integrates missing view recovery and common representation learning. **IMSC-AGL** [34] combines graph learning, spectral constraint, and regularization to capture cross-view consistency. **BGI-MVSC** (https://github.com/ckghostwj/NN2023_BGIMVSC) [35] integrates adaptive weighted consensus graph learning and balanced spectral clustering. **IMVTSC-MVI** (https://github.com/DarrenZZhang/AAAI21-IMVTSC-MVI) [27] utilizes missing view inference, similarity graph learning, consistency constraint, and low-rank tensor constraint.

Subspace-based methods: **IMSR** (https://github.com/liujiyuan13/IMSR-code_release) [36] enhances clustering performance by jointly integrating missing-view imputation with self-representation learning to adjust subspace learning. This unified approach effectively leverages latent information even when handling incomplete multi-view data, thereby improving clustering accuracy under view-missing scenarios.

Anchor-based methods: Anchor graph learning is often employed to handle large-scale multi-view data efficiently by reducing complexity. **SIMVC-SA** (https://github.com/wy1019/SIMVC-SA) [37] specifically addresses the Anchor-Unaligned Problem for Incomplete Data. It constructs view-specific anchor graphs to capture complementary information and introduces a novel structure alignment module to refine the cross-view anchor correspondence.

Uncoupling methods: **T-UMC** (https://github.com/AllminerLab/Code-for-T-UMC-master) [16] selects reliable views using VSSC, couples views through cross-view coupling, preserves local geometry, and explores high-order correlations via the TNN. **MVC-UM** (https://github.com/yuhongcqupt/MVC-UM) [15] combines matrix decomposition, cross-view mapping loss, and local structure constraint. Since these two methods are designed to handle complete datasets, during the experiment, the method of mean imputation is adopted to deal with the missing samples.

4.4. Evaluation Metrics

Five evaluation metrics [38] are utilized to evaluate the clustering performance, including accuracy (ACC), normalized mutual information (NMI), purity, Fscore, and precision. Higher evaluation indicators indicate better clustering performance of the model.

4.5. Parameter Settings

The source codes of all the compared methods have been released by their respective authors, and their parameters are adjusted within the recommended ranges. The detailed parameter configurations of the nine compared methods are presented in Tables 5–9. For the proposed model, λ_1 is in [0.01, 0.05, 0.1, 0.5, 1], and λ_2 is in [1e-5, 1e-4, 1e-3, 1e-2, 1e-1].

Theoretically, k needs to be large enough to encompass the information required to distinguish between different clusters, so it typically should be greater than or equal to the true number of categories in the dataset. However, an excessively large k value may retain too much redundant information or even noise, while also increasing the computational complexity of subsequent steps. In this experiment, we set the reduced-dimension k to 20 and choose to use the view with the minimum missing rate as the best view.

To more systematically evaluate the impact of k on the clustering performance and provide a justification for our choice, we conduct a series of supplementary experiments. We test the effects of different k values on five key clustering evaluation metrics across two representative datasets. The experimental results are plotted in Figure 3. As shown in the figure, when $k = 20$, two representative datasets achieve promising clustering performance.

Table 5. Parameter settings on the Yale dataset.

Parameter	UEAF	IMSR	T-UMC	MVC-UM	HCLS-CGL	IMSC-AGL	SIMVC	BGVI-MVSC	IMVTSC-MVI
Parameter 1	0.100	1.000	0.300	10^{-3}	2.000	0.100	10^{-2}	7.000	10^{-5}
Parameter 2	10^{-2}	0.250	0.800	10^{2}	10^{-4}	10^{3}	10^{-4}	0.100	10^{-2}
Parameter 3	10^{-5}	-	0.300	10^{2}	10^{-3}	10^{2}	15.000	10.000	10^{-2}

Table 6. Parameter settings on the YaleA dataset.

Parameter	UEAF	IMSR	T-UMC	MVC-UM	HCLS-CGL	IMSC-AGL	SIMVC	BGVI-MVSC	IMVTSC-MVI
Parameter 1	0.1	0.0039	0.3	10^{-3}	2	0.1	10^{-2}	7	10^{-5}
Parameter 2	10^{-2}	0.0039	0.8	10^{2}	10^{-4}	10^{3}	1	0.1	10^{-2}
Parameter 3	10^{-5}	-	0.3	10^{2}	10^{-3}	10^{2}	15	10	10^{-2}

Table 7. Parameter settings on the BBCSport dataset.

Parameter	UEAF	IMSR	T-UMC	MVC-UM	HCLS-CGL	IMSC-AGL	SIMVC	BGVI-MVSC	IMVTSC-MVI
Parameter 1	0.1	1	0.5	10^{-3}	2	0.1	10^{-2}	7	10^{-5}
Parameter 2	10^{-2}	0.0039	0.3	10^{2}	10^{-4}	10^{3}	1	1	10^{-2}
Parameter 3	10^{-5}	-	0.5	10^{2}	10^{-3}	10^{2}	5	1	10^{-2}

Table 8. Parameter settings on the COIL20 dataset.

Parameter	UEAF	IMSR	T-UMC	MVC-UM	HCLS-CGL	IMSC-AGL	SIMVC	BGVI-MVSC	IMVTSC-MVI
Parameter 1	0.1	0.0039	0.5	10^{-3}	2	0.1	1	7	10^{-5}
Parameter 2	10^{-2}	0.0156	0.3	10^{2}	10^{-4}	10^{3}	10^{-2}	0.1	10^{-2}
Parameter 3	10^{-5}	-	0.5	10^{2}	10^{-3}	10^{2}	20	10	10^{-2}

Table 9. Parameter settings on the ORL dataset.

Parameter	UEAF	IMSR	T-UMC	MVC-UM	HCLS-CGL	IMSC-AGL	SIMVC	BGVI-MVSC	IMVTSC-MVI
Parameter 1	0.1	0.0625	0.5	10^{-3}	2	0.1	10^{-2}	7	10^{-5}
Parameter 2	10^{-2}	1	0.3	10^{2}	10^{-4}	10^{3}	1	0.1	10^{-2}
Parameter 3	10^{-5}	-	0.5	10^{2}	10^{-3}	10^{2}	40	10	10^{-2}

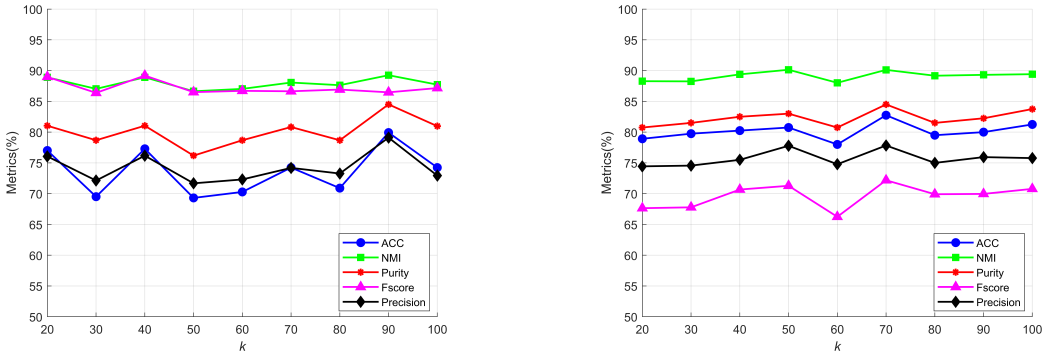

Figure 3. Results of evaluation indicators under different values of k.

4.6. Experimental Results

To make the comparative experiment more convincing, we run ten experiments on the same uncoupled and incomplete dataset for all the methods. We take their average values and standard deviations as references, and the specific results are shown in Tables 10–14. The best results are highlighted in bold. From the experimental results, we make the following observations.

Overall, the proposed model outperforms nine existing methods on the five datasets, including two methods for handling uncoupled data and seven methods for handling incomplete data. This demonstrates the ability of the proposed method to handle uncoupled and incomplete data. The specific performance is as follows:

- The experiments are tested on five real-world datasets, and the results suggest that the model outperforms nine existing multi-view clustering methods in most cases, including two for coupled data and seven for uncoupled data. Specifically, in terms of ACC, NMI, purity, Fscore, and precision, TUIMC performed well.
- Comparison with graph-based methods: The proposed method achieves outstanding clustering results in five evaluation metrics on the five datasets. Essentially, all the metrics are higher than those of the comparison methods. For example, on the Yale dataset with a missing rate of 0.1, the ACC, NMI, and purity of the proposed method

are 36.97%, 30.75%, and 35.87% higher than those of HCLS-CGL, respectively. Comparison with anchor-based methods: On the five datasets, all metrics are higher than those of SIMVC. For example, on the ORL dataset with a missing rate of 0.1, the ACC, NMI, and purity of the proposed model are, respectively, 24.09%, 19.04%, and 24.28% higher than those of SIMVC. Comparison with subspace-based methods: On the five datasets, all the metrics are higher than those of IMSR. This demonstrates that the proposed method exhibits superior performance compared to alignment-oriented approaches.

- Comparison with uncoupled methods: On the COIL20 dataset with a missing rate of 0.3, the ACC, NMI, and purity are, respectively, 3.91%, 6.87%, and 6.39% higher than those of T-UMC. For MVC-UM, all the metrics for TUIMC are higher than MVC-UM's corresponding metrics. This indicates that the proposed method still maintains superiority compared to the uncoupled methods, likely due to the fact that these uncoupled methods do not specifically address the challenges of incomplete data.

4.7. Analysis of Running Time

To compare the runtime efficiency of different models, we calculate the average running time for all methods across five benchmark datasets. The detailed results are presented in Table 15. As illustrated in the figure, our model exhibits moderate runtime performance, primarily due to the matrix inversion operation in the proposed algorithm, which introduces a computational complexity of $O(N^3)$.

4.8. Parameter Sensitivity

There are two parameters that can be adjusted: λ_1 and λ_2. We let λ_1 traverse the grid across the values $[0.01, 0.05, 0.1, 0.5, 1]$ and λ_2 across the values $[10^{-5}, 10^{-4}, 10^{-3}, 10^{-2}, 10^{-1}]$ to observe the changes in ACC performance of the proposed model with a 10% missing rate. As shown in Figure 4, it can be seen that different datasets exhibit varying degrees of sensitivity to λ_1 and λ_2. However, for most datasets, the clustering performance is satisfactory when $\lambda_1 \in [0.01, 0.1, 0.5]$ and $\lambda_2 \in [10^{-5}, 10^{-4}, 10^{-3}]$. All the above results are obtained under the condition that the dimensionality reduction number $k = 20$.

Table 10. Experimental results (mean% ± standard deviation%) on the Yale dataset.

m	Metric	UEAF	IMSR	T-UMC	MVC-UM	HCLS-CGL	IMSC-AGL	SIMVC	BGVI-MVSC	IMVTSC-MVI	Ours
0.1	ACC	21.27 ± 0.69	32.00 ± 1.78	58.12 ± 1.35	55.15 ± 2.27	39.45 ± 1.29	43.03 ± 0.00	39.27 ± 0.42	26.67 ± 0.00	47.94 ± 0.04	**76.42 ± 0.73**
	NMI	23.83 ± 1.72	36.61 ± 1.39	61.71 ± 1.08	60.52 ± 1.67	43.64 ± 1.20	45.84 ± 0.00	43.10 ± 0.31	29.96 ± 0.00	50.61 ± 0.02	**74.39 ± 0.83**
	Purity	22.73 ± 0.84	33.45 ± 1.98	59.15 ± 1.35	55.88 ± 2.04	40.55 ± 0.00	45.45 ± 0.00	41.21 ± 0.45	28.48 ± 0.00	49.03 ± 0.03	**76.42 ± 0.73**
	Fscore	10.82 ± 1.50	16.19 ± 1.68	45.16 ± 1.29	44.38 ± 0.00	23.16 ± 0.84	24.36 ± 0.00	20.47 ± 0.00	11.27 ± 1.30	29.90 ± 0.03	**61.85 ± 1.35**
	Precision	8.23 ± 0.37	15.19 ± 1.50	42.60 ± 1.49	40.71 ± 2.43	21.94 ± 1.11	23.90 ± 0.00	22.76 ± 0.21	10.00 ± 0.00	28.84 ± 0.02	**60.89 ± 0.01**
0.2	ACC	18.18 ± 0.49	36.06 ± 2.87	59.52 ± 1.42	52.91 ± 2.32	57.03 ± 1.55	41.82 ± 0.00	35.81 ± 0.59	26.88 ± 0.00	44.03 ± 0.02	**72.12 ± 0.49**
	NMI	19.85 ± 0.43	41.46 ± 2.19	62.77 ± 0.61	59.94 ± 2.22	54.92 ± 1.10	47.03 ± 0.00	39.56 ± 0.26	29.51 ± 0.00	47.04 ± 0.01	**70.60 ± 0.87**
	Purity	19.33 ± 0.61	37.82 ± 2.68	60.00 ± 1.50	40.60 ± 0.00	84.90 ± 0.00	79.00 ± 0.00	36.67 ± 0.00	30.30 ± 0.00	45.27 ± 0.01	**72.18 ± 0.34**
	Fscore	13.81 ± 1.28	20.19 ± 2.54	47.48 ± 1.16	43.32 ± 3.36	36.74 ± 1.57	26.06 ± 0.00	17.56 ± 0.97	31.52 ± 0.00	26.27 ± 0.01	**55.77 ± 0.12**
	Precision	8.06 ± 0.08	19.45 ± 2.40	44.82 ± 1.02	39.95 ± 2.88	33.67 ± 0.97	24.59 ± 0.00	19.47 ± 0.08	16.49 ± 0.00	25.37 ± 0.01	**54.80 ± 1.61**
0.3	ACC	18.06 ± 0.56	35.82 ± 1.60	57.52 ± 0.67	50.30 ± 3.14	52.73 ± 2.02	46.67 ± 0.00	32.97 ± 0.37	25.30 ± 0.00	39.09 ± 0.02	**68.48 ± 2.46**
	NMI	18.31 ± 1.00	40.11 ± 1.21	61.20 ± 0.58	58.15 ± 2.22	54.26 ± 1.35	47.80 ± 0.00	36.30 ± 0.12	27.82 ± 0.00	40.04 ± 0.01	**68.40 ± 1.14**
	Purity	19.70 ± 0.59	37.52 ± 1.78	58.67 ± 0.56	51.39 ± 2.80	53.94 ± 2.21	48.48 ± 0.00	34.78 ± 0.01	23.33 ± 0.00	40.06 ± 0.01	**68.61 ± 2.35**
	Fscore	20.38 ± 1.63	18.99 ± 1.45	45.21 ± 1.06	41.27 ± 2.43	35.44 ± 0.02	28.61 ± 0.00	15.40 ± 0.87	17.03 ± 0.00	20.47 ± 0.01	**52.04 ± 1.92**
	Precision	9.29 ± 5.98	18.26 ± 1.39	42.67 ± 0.82	37.44 ± 2.51	32.47 ± 1.67	27.10 ± 0.00	17.43 ± 0.29	17.41 ± 0.00	19.31 ± 0.01	**50.54 ± 1.40**
0.4	ACC	18.67 ± 0.88	49.15 ± 1.14	54.18 ± 0.91	51.09 ± 2.97	58.36 ± 0.57	49.70 ± 0.00	26.82 ± 0.78	24.48 ± 0.00	31.27 ± 0.03	**66.85 ± 1.14**
	NMI	17.31 ± 0.93	52.18 ± 0.91	59.18 ± 0.56	57.54 ± 1.91	56.78 ± 0.49	54.55 ± 0.00	33.59 ± 0.58	23.64 ± 0.00	34.58 ± 0.03	**66.47 ± 1.16**
	Purity	20.12 ± 0.80	50.30 ± 1.28	55.33 ± 0.64	51.76 ± 2.94	58.61 ± 0.41	51.52 ± 0.00	28.72 ± 1.13	29.70 ± 0.00	32.36 ± 0.03	**66.58 ± 1.26**
	Fscore	14.28 ± 1.28	19.29 ± 1.82	41.91 ± 0.93	38.27 ± 2.48	35.17 ± 0.44	29.27 ± 0.00	10.94 ± 0.24	16.36 ± 0.00	14.38 ± 0.02	**52.09 ± 1.83**
	Precision	9.87 ± 1.10	22.18 ± 2.11	41.06 ± 0.80	38.51 ± 2.17	36.52 ± 0.52	30.16 ± 0.00	13.64 ± 0.19	12.44 ± 0.00	13.64 ± 0.02	**51.39 ± 1.35**
0.5	ACC	18.15 ± 0.79	50.95 ± 0.52	54.21 ± 0.58	55.19 ± 3.42	62.62 ± 0.87	46.61 ± 0.00	20.06 ± 0.02	28.85 ± 0.00	29.89 ± 0.02	**67.57 ± 0.98**
	NMI	17.11 ± 0.85	52.13 ± 0.70	57.12 ± 0.84	56.97 ± 2.11	62.32 ± 0.35	54.97 ± 0.00	20.61 ± 0.17	28.80 ± 0.00	34.68 ± 0.02	**69.25 ± 1.11**
	Purity	20.86 ± 0.57	49.32 ± 0.74	56.34 ± 0.87	54.47 ± 3.10	62.23 ± 0.73	55.80 ± 0.00	21.70 ± 0.12	29.09 ± 0.00	30.97 ± 0.02	**69.58 ± 0.82**
	Fscore	16.95 ± 1.02	20.38 ± 1.40	44.16 ± 1.15	40.97 ± 2.74	36.50 ± 0.71	30.72 ± 0.00	6.48 ± 0.02	24.00 ± 0.00	14.51 ± 0.02	**52.52 ± 1.38**
	Precision	9.76 ± 0.48	22.60 ± 2.01	43.24 ± 1.40	40.16 ± 2.43	38.15 ± 0.52	30.49 ± 0.00	11.96 ± 0.02	12.91 ± 0.00	13.73 ± 0.02	**50.55 ± 1.31**

Table 11. Experimental results (mean% ± standard deviation%) on the YaleA dataset.

m	Metric	UEAF	IMSR	T-UMC	MVC-UM	HCLS-CGL	IMSC-AGL	SIMVC	BGVI-MVSC	IMVTSC-MVI	Ours
0.1	ACC	19.45 ± 0.04	72.85 ± 2.57	78.42 ± 4.84	23.94 ± 1.67	26.79 ± 0.08	45.45 ± 0.00	73.57 ± 0.57	30.91 ± 0.00	80.12 ± 0.01	**93.93 ± 0.19**
	NMI	21.37 ± 0.35	76.22 ± 1.57	80.48 ± 3.52	28.47 ± 2.26	29.94 ± 0.52	48.75 ± 0.00	75.91 ± 0.42	34.76 ± 0.00	85.06 ± 0.00	**91.83 ± 0.27**
	Purity	20.18 ± 0.33	73.82 ± 2.46	78.91 ± 4.73	26.06 ± 1.43	27.58 ± 0.87	48.48 ± 0.00	74.67 ± 0.45	32.12 ± 0.00	82.55 ± 0.00	**93.39 ± 0.19**
	Fscore	7.00 ± 0.00	63.25 ± 2.51	70.41 ± 5.48	11.98 ± 1.45	10.36 ± 0.41	29.45 ± 0.00	60.25 ± 0,21	13.94 ± 0.00	82.73 ± 0.01	**87.61 ± 0.31**
	Precision	5.97 ± 0.07	61.97 ± 2.33	68.05 ± 4.95	10.11 ± 1.22	9.98 ± 0.35	28.19 ± 0.00	63.37 ± 0.89	13.14 ± 0.00	79.18 ± 0.01	**86.41 ± 0.49**
0.2	ACC	18.18 ± 0.00	73.09 ± 0.65	80.30 ± 4.32	23.64 ± 1.11	33.58 ± 1.83	52.12 ± 0.00	70.09 ± 0.47	31.52 ± 0.00	76.67 ± 2.18	**92.48 ± 0.71**
	NMI	17.85 ± 0.42	74.33 ± 1.18	82.23 ± 1.74	28.03 ± 1.26	37.23 ± 1.88	54.89 ± 0.00	74.53 ± 0.53	39.26 ± 0.00	91.39 ± 1.85	**90.96 ± 0.83**
	Purity	19.39 ± 0.00	73.39 ± 0.83	80.73 ± 4.02	26.48 ± 1.11	34.79 ± 1.67	53.33 ± 0.00	72.02 ± 0.46	36.97 ± 0.00	87.73 ± 2.86	**92.48 ± 0.71**
	Fscore	15.56 ± 1.04	61.39 ± 1.48	72.93 ± 2.86	12.81 ± 1.37	16.93 ± 1.79	37.09 ± 0.00	58.77 ± 0.32	21.58 ± 0.00	85.73 ± 4.03	**85.98 ± 1.06**
	Precision	8.17 ± 0.01	60.31 ± 1.42	70.43 ± 2.88	10.39 ± 0.81	16.01 ± 1.82	35.52 ± 0.00	61.92 ± 0.27	18.03 ± 0.00	83.24 ± 3.37	**84.48 ± 2.04**
0.3	ACC	21.21 ± 0.00	74.06 ± 1.51	73.27 ± 2.28	21.27 ± 0.64	38.97 ± 2.04	52.12 ± 0.00	60.85 ± 0.33	29.09 ± 0.00	74.12 ± 0.01	**89.39 ± 0.32**
	NMI	24.43 ± 0.25	77.85 ± 1.77	77.44 ± 1.73	22.41 ± 1.18	41.47 ± 1.02	52.84 ± 0.00	65.14 ± 0.47	36.07 ± 0.00	81.44 ± 0.02	**86.33 ± 0.47**
	Purity	21.82 ± 0.00	74.48 ± 1.60	73.94 ± 2.23	21.94 ± 0.63	40.61 ± 0.63	53.33 ± 0.00	62.74 ± 0.19	33.33 ± 0.00	77.88 ± 0.03	**89.39 ± 0.32**
	Fscore	14.78 ± 0.03	65.54 ± 3.03	65.37 ± 2.02	9.07 ± 0.88	21.04 ± 1.15	33.32 ± 0.00	44.41 ± 0.12	16.24 ± 0.00	75.85 ± 0.03	**80.61 ± 0.83**
	Precision	9.35 ± 0.02	63.48 ± 2.62	63.42 ± 1.61	7.31 ± 0.53	20.00 ± 1.07	32.33 ± 0.00	47.85 ± 0.22	14.33 ± 0.00	73.96 ± 0.03	**75.90 ± 0.42**
0.4	ACC	17.03 ± 0.04	70.42 ± 2.04	69.33 ± 1.77	20.24 ± 0.59	51.39 ± 2.23	53.94 ± 0.00	57.63 ± 0.32	22.42 ± 0.00	70.73 ± 0.05	**84.06 ± 1.03**
	NMI	16.00 ± 0.04	73.19 ± 1.76	75.33 ± 1.51	22.41 ± 0.82	53.52 ± 1.23	57.78 ± 0.00	61.68 ± 0.27	25.04 ± 0.00	78.47 ± 0.03	**81.91 ± 0.97**
	Purity	17.63 ± 0.04	71.09 ± 0.02	69.76 ± 1.84	21.70 ± 0.56	53.39 ± 2.13	56.36 ± 0.00	59.03 ± 0.24	22.42 ± 0.00	73.88 ± 0.04	**84.06 ± 1.03**
	Fscore	52.36 ± 0.00	59.03 ± 2.42	63.18 ± 2.50	13.48 ± 0.38	33.81 ± 1.33	38.91 ± 0.00	41.34 ± 0.38	22.06 ± 0.00	72.11 ± 0.04	**72.86 ± 1.35**
	Precision	10.88 ± 0.00	58.26 ± 2.55	60.06 ± 2.46	8.78 ± 0.23	31.43 ± 1.39	37.97 ± 0.00	44.63 ± 0.35	10.46 ± 0.00	77.96 ± 0.04	**67.59 ± 1.15**
0.5	ACC	20.85 ± 0.59	69.82 ± 4.39	69.64 ± 4.02	21.15 ± 1.79	60.61 ± 1.03	66.06 ± 0.00	32.02 ± 0.28	23.64 ± 0.00	62.61 ± 0.03	**83.64 ± 2.78**
	NMI	15.94 ± 0.06	72.54 ± 4.40	75.22 ± 2.95	24.37 ± 2.72	60.08 ± 1.12	67.02 ± 0.00	36.75 ± 0.32	26.53 ± 0.00	75.09 ± 0.02	**82.39 ± 1.11**
	Purity	21.57 ± 0.26	70.61 ± 4.71	70.00 ± 3.84	21.52 ± 1.81	61.76 ± 1.05	67.88 ± 0.00	33.21 ± 0.27	24.85 ± 0.00	68.18 ± 0.03	**84.00 ± 2.04**
	Fscore	18.56 ± 0.94	58.50 ± 6.05	62.86 ± 4.07	24.07 ± 0.96	42.69 ± 1.26	52.73 ± 0.00	15.48 ± 0.32	20.48 ± 0.00	64.28 ± 0.04	**72.87 ± 1.87**
	Precision	9.61 ± 0.11	56.72 ± 5.89	59.84 ± 4.12	12.12 ± 1.11	40.85 ± 1.06	50.67 ± 0.00	18.71 ± 0.13	12.54 ± 0.00	59.56 ± 0.03	**66.76 ± 1.78**

Table 12. Experimental results (mean% ± standard deviation%) on the BBCSport dataset.

m	Metric	UEAF	IMSR	T-UMC	MVC-UM	HCLS-CGL	IMSC-AGL	SIMVC	BGVI-MVSC	IMVTSC-MVI	Ours
0.1	ACC	49.81 ± 0.25	60.51 ± 0.12	92.35 ± 2.88	40.02 ± 4.23	38.69 ± 0.22	79.23 ± 0.00	66.52 ± 0.91	40.63 ± 0.00	77.32 ± 0.00	**93.49 ± 0.09**
	NMI	19.18 ± 0.11	33.73 ± 0.23	79.64 ± 3.73	8.54 ± 3.74	12.71 ± 0.26	53.43 ± 0.00	34.41 ± 0.28	9.56 ± 0.00	69.93 ± 0.00	**83.64 ± 0.31**
	Purity	56.41 ± 0.21	67.70 ± 0.17	92.35 ± 2.88	42.17 ± 3.56	46.60 ± 0.02	79.23 ± 0.00	66.52 ± 0.88	47.79 ± 0.00	80.51 ± 0.00	**93.49 ± 0.09**
	Fscore	35.78 ± 0.21	45.99 ± 0.17	85.93 ± 3.24	59.89 ± 12.16	28.85 ± 0.23	60.63 ± 0.00	52.85 ± 0.57	44.86 ± 0.00	64.82 ± 0.00	85.60 ± 0.09
	Precision	37.32 ± 0.21	49.45 ± 0.18	86.37 ± 3.24	37.22 ± 1.99	30.20 ± 0.33	65.16 ± 0.00	46.67 ± 0.45	33.74 ± 0.00	68.75 ± 0.00	**86.60 ± 0.07**
0.2	ACC	51.82 ± 0.17	62.06 ± 0.42	90.66 ± 0.84	40.63 ± 4.10	42.68 ± 0.31	77.94 ± 0.00	64.40 ± 0.54	42.28 ± 0.00	70.96 ± 0.00	**92.83 ± 0.19**
	NMI	20.09 ± 0.22	35.98 ± 0.19	74.51 ± 1.54	8.94 ± 0.20	18.98 ± 0.08	50.29 ± 0.00	32.46 ± 0.24	15.04 ± 0.00	56.00 ± 0.00	**78.91 ± 0.61**
	Purity	51.82 ± 0.17	64.06 ± 0.10	90.66 ± 0.84	42.90 ± 2.57	52.19 ± 0.06	77.94 ± 0.00	64.47 ± 0.53	51.10 ± 0.00	76.47 ± 1.70	**92.83 ± 0.19**
	Fscore	33.82 ± 0.23	43.94 ± 0.38	84.88 ± 0.63	55.96 ± 13.47	40.50 ± 0.11	59.34 ± 0.00	51.58 ± 0.21	43.85 ± 0.00	61.24 ± 0.00	**85.23 ± 0.27**
	Precision	36.20 ± 0.22	47.87 ± 0.33	82.86 ± 1.31	35.82 ± 2.46	36.10 ± 0.07	63.40 ± 0.00	44.28 ± 0.33	35.93 ± 0.00	63.00 ± 0.00	**86.39 ± 0.94**
0.3	ACC	40.75 ± 0.93	54.08 ± 0.71	88.49 ± 0.41	41.23 ± 5.33	63.68 ± 0.38	62.87 ± 0.00	62.40 ± 0.39	41.73 ± 0.00	68.09 ± 0.00	**90.72 ± 0.01**
	NMI	12.57 ± 0.58	33.49 ± 0.83	69.54 ± 0.85	9.20 ± 0.05	39.90 ± 0.32	40.24 ± 0.00	30.63 ± 0.27	21.79 ± 0.00	48.41 ± 0.00	**78.16 ± 0.50**
	Purity	46.48 ± 0.47	60.22 ± 0.51	88.49 ± 0.41	42.85 ± 4.75	67.30 ± 0.32	69.30 ± 1.70	61.32 ± 0.22	46.32 ± 0.00	68.09 ± 0.00	**90.72 ± 0.10**
	Fscore	28.67 ± 0.46	43.22 ± 0.76	**83.96 ± 0.29**	66.89 ± 1.30	49.41 ± 0.45	53.31 ± 0.00	49.84 ± 0.49	39.50 ± 0.00	52.66 ± 0.00	80.66 ± 0.20
	Precision	30.37 ± 0.56	44.02 ± 0.64	79.83 ± 0.82	38.29 ± 0.27	51.27 ± 0.37	54.98 ± 0.00	41.09 ± 0.42	36.86 ± 0.00	56.68 ± 0.00	**81.87 ± 0.26**
0.4	ACC	25.91 ± 0.00	49.78 ± 0.59	88.25 ± 1.55	44.49 ± 3.68	57.68 ± 1.23	70.22 ± 0.00	47.93 ± 0.09	41.10 ± 0.00	66.40 ± 0.00	**89.06 ± 2.62**
	NMI	1.41 ± 0.00	27.20 ± 5.42	68.90 ± 0.30	11.53 ± 4.98	32.88 ± 0.27	39.21 ± 0.00	32.82 ± 0.42	10.97 ± 0.00	58.28 ± 0.00	**72.87 ± 3.40**
	Purity	36.03 ± 0.00	54.76 ± 4.92	88.25 ± 1.55	46.25 ± 3.88	61.10 ± 0.18	70.22 ± 0.00	49.21 ± 0.39	44.60 ± 0.00	74.89 ± 0.00	**89.06 ± 2.62**
	Fscore	25.72 ± 0.00	40.86 ± 4.37	78.75 ± 1.81	75.06 ± 1.01	47.54 ± 1.06	50.19 ± 0.00	31.50 ± 0.71	29.10 ± 0.00	58.51 ± 0.00	**79.19 ± 0.65**
	Precision	24.62 ± 0.00	40.11 ± 4.21	78.97 ± 2.44	40.12 ± 1.92	45.39 ± 0.66	52.88 ± 0.00	22.75 ± 0.82	28.25 ± 0.00	63.33 ± 0.00	**79.78 ± 0.54**
0.5	ACC	27.21 ± 0.00	34.65 ± 2.28	86.14 ± 1.00	45.39 ± 5.96	72.98 ± 0.00	79.41 ± 0.00	45.81 ± 0.12	39.71 ± 0.00	62.17 ± 0.00	**87.21 ± 0.09**
	NMI	9.24 ± 0.05	39.20 ± 0.93	68.78 ± 0.83	11.82 ± 5.37	42.19 ± 0.03	51.41 ± 0.00	31.65 ± 0.37	15.10 ± 0.00	42.89 ± 0.00	**72.23 ± 0.32**
	Purity	35.47 ± 0.00	38.64 ± 1.13	86.14 ± 1.00	46.21 ± 5.79	72.98 ± 0.00	79.41 ± 0.00	47.89 ± 0.23	42.46 ± 0.00	62.17 ± 0.00	**87.21 ± 0.09**
	Fscore	32.66 ± 2.89	45.84 ± 4.84	74.38 ± 1.00	**77.35 ± 0.87**	61.56 ± 0.08	61.68 ± 0.00	31.09 ± 0.38	48.29 ± 0.00	47.42 ± 0.00	75.49 ± 0.21
	Precision	27.33 ± 1.66	33.03 ± 1.39	**78.08 ± 0.76**	40.62 ± 2.18	56.82 ± 0.05	64.06 ± 0.00	18.72 ± 0.43	37.58 ± 0.00	50.82 ± 0.00	75.38 ± 1.10

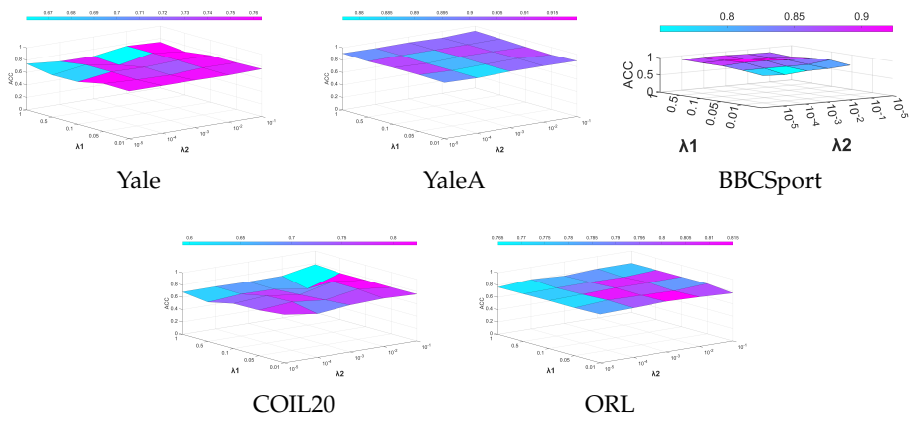

Figure 4. Clustering performance (ACC) on datasets with different values for λ_1 and λ_2.

Table 13. Experimental results (mean% ± standard deviation%) on the COIL20 dataset.

m	Metric	UEAF	IMSR	T-UMC	MVC-UM	HCLS-CGL	IMSC-AGL	SIMVC	BGVI-MVSC	IMVTSC-MVI	Ours
0.1	ACC	10.94 ± 0.26	15.77 ± 0.67	**75.45 ± 1.67**	34.63 ± 2.73	21.90 ± 0.63	23.19 ± 0.00	19.90 ± 0.61	15.69 ± 0.00	16.93 ± 0.00	75.38 ± 1.39
	NMI	6.64 ± 0.43	10.99 ± 0.75	83.09 ± 0.77	46.00 ± 2.26	22.53 ± 0.52	16.75 ± 0.00	16.37 ± 0.75	11.33 ± 0.00	14.01 ± 0.00	**88.13 ± 0.79**
	Purity	11.45 ± 0.29	16.69 ± 0.71	76.31 ± 0.96	35.50 ± 2.47	24.53 ± 0.59	25.21 ± 0.00	20.41 ± 0.55	6.94 ± 0.00	17.42 ± 0.00	**80.90 ± 0.14**
	Fscore	7.43 ± 0.33	8.21 ± 0.35	74.20 ± 0.88	33.95 ± 2.41	12.53 ± 0.25	12.81 ± 0.00	10.77 ± 0.85	13.18 ± 0.00	8.62 ± 0.00	**87.79 ± 1.23**
	Precision	6.45 ± 0.13	7.88 ± 0.36	71.46 ± 1.43	30.55 ± 1.88	12.04 ± 0.25	12.31 ± 0.00	11.17 ± 0.33	2.80 ± 0.00	8.93 ± 0.00	**74.34 ± 1.92**
0.2	ACC	9.18 ± 0.12	30.11 ± 0.60	72.24 ± 2.93	20.56 ± 1.22	25.67 ± 0.96	28.40 ± 0.00	17.15 ± 0.20	16.74 ± 0.00	19.58 ± 0.00	**75.88 ± 2.35**
	NMI	4.38 ± 0.13	24.93 ± 0.84	79.71 ± 1.71	29.61 ± 1.56	27.42 ± 0.84	24.29 ± 0.00	13.52 ± 0.48	11.05 ± 0.00	18.41 ± 0.00	**87.34 ± 0.74**
	Purity	9.57 ± 0.11	30.97 ± 0.58	72.78 ± 2.83	21.96 ± 1.20	28.67 ± 0.86	31.94 ± 0.00	17.79 ± 0.94	6.98 ± 0.00	21.25 ± 0.00	**80.42 ± 1.43**
	Fscore	15.44 ± 0.08	18.50 ± 0.58	71.35 ± 0.21	17.62 ± 1.60	15.81 ± 0.48	17.35 ± 0.00	8.99 ± 0.75	8.64 ± 0.00	10.50 ± 0.00	**85.39 ± 1.33**
	Precision	7.43 ± 0.14	17.90 ± 0.59	68.15 ± 2.48	15.61 ± 1.06	14.86 ± 0.63	16.66 ± 0.00	9.51 ± 0.55	2.40 ± 0.00	10.29 ± 0.00	**74.52 ± 1.50**
0.3	ACC	8.86 ± 0.14	40.13 ± 2.28	73.10 ± 0.14	20.69 ± 0.63	31.66 ± 1.08	29.58 ± 0.00	16.50 ± 0.32	17.08 ± 0.00	19.97 ± 0.00	**77.01 ± 0.50**
	NMI	5.05 ± 0.19	39.19 ± 2.30	79.12 ± 0.45	30.86 ± 1.03	35.11 ± 0.55	25.10 ± 0.00	13.57 ± 0.99	11.39 ± 0.00	18.65 ± 0.00	**85.99 ± 0.67**
	Purity	9.13 ± 0.12	40.88 ± 2.29	73.43 ± 0.18	21.92 ± 0.68	35.59 ± 0.96	33.61 ± 0.00	17.15 ± 0.14	6.44 ± 0.00	21.19 ± 0.00	**79.82 ± 1.38**
	Fscore	30.56 ± 0.67	29.90 ± 1.95	72.82 ± 0.65	17.07 ± 0.85	21.56 ± 0.71	17.57 ± 0.00	8.87 ± 0.88	14.26 ± 0.00	10.81 ± 0.00	**82.16 ± 0.92**
	Precision	8.50 ± 0.60	28.04 ± 2.12	68.98 ± 0.56	15.39 ± 0.71	19.30 ± 0.61	16.68 ± 0.00	9.79 ± 0.98	2.22 ± 0.00	10.50 ± 0.00	**73.89 ± 1.92**
0.4	ACC	8.08 ± 0.08	49.02 ± 3.02	66.71 ± 2.19	23.12 ± 0.67	35.76 ± 0.70	27.64 ± 0.00	20.00 ± 0.94	13.54 ± 0.00	24.71 ± 0.00	**67.95 ± 1.01**
	NMI	4.56 ± 0.13	48.64 ± 2.94	74.58 ± 1.31	34.31 ± 0.85	40.54 ± 0.41	23.60 ± 0.00	18.88 ± 0.47	9.21 ± 0.00	24.08 ± 0.00	**81.90 ± 1.31**
	Purity	8.40 ± 0.14	49.51 ± 3.15	68.21 ± 2.14	24.73 ± 0.49	41.44 ± 0.78	30.90 ± 0.00	20.48 ± 0.49	5.65 ± 0.00	27.92 ± 0.00	**73.59 ± 0.77**
	Fscore	52.35 ± 0.06	38.71 ± 3.41	66.03 ± 1.15	18.75 ± 0.96	27.63 ± 0.74	15.34 ± 0.00	12.24 ± 0.75	24.55 ± 0.00	14.90 ± 0.00	**76.98 ± 1.70**
	Precision	9.01 ± 0.00	36.02 ± 3.36	62.57 ± 1.60	17.15 ± 0.65	23.57 ± 0.34	14.96 ± 0.00	14.35 ± 0.34	1.27 ± 0.00	14.25 ± 0.00	**64.06 ± 3.20**
0.5	ACC	6.85 ± 0.09	53.97 ± 1.05	64.31 ± 2.23	27.90 ± 1.25	35.34 ± 1.32	35.97 ± 0.00	20.05 ± 0.07	10.69 ± 0.00	20.43 ± 0.00	**66.31 ± 2.86**
	NMI	3.51 ± 0.34	52.57 ± 0.34	**72.99 ± 1.50**	39.83 ± 1.16	41.10 ± 0.81	35.66 ± 0.00	23.03 ± 0.70	6.96 ± 0.00	19.70 ± 0.00	77.32 ± 2.25
	Purity	6.95 ± 0.06	54.71 ± 1.06	66.53 ± 2.25	29.28 ± 1.47	39.71 ± 1.03	40.13 ± 0.00	20.62 ± 0.21	5.17 ± 0.00	23.86 ± 0.00	**72.26 ± 1.85**
	Fscore	**80.99 ± 0.46**	43.37 ± 0.76	63.62 ± 1.20	23.48 ± 0.59	26.78 ± 0.60	25.73 ± 0.00	14.72 ± 0.82	23.05 ± 0.00	7.60 ± 0.00	72.14 ± 1.84
	Precision	9.29 ± 0.05	40.22 ± 0.72	**59.85 ± 1.81**	21.25 ± 0.48	23.73 ± 0.68	24.52 ± 0.00	0.47 ± 0.00	9.71 ± 0.00	6.50 ± 0.00	58.70 ± 0.36

Table 14. Experimental results (mean% ± standard deviation%) on the ORL dataset.

m	Metric	UEAF	IMSR	T-UMC	MVC-UM	HCLS-CGL	IMSC-AGL	SIMVC	BGVI-MVSC	IMVTSC-MVI	Ours
0.1	ACC	15.20 ± 0.43	73.70 ± 2.71	75.65 ± 1.71	15.58 ± 0.68	35.34 ± 1.32	46.75 ± 0.00	55.05 ± 0.78	27.75 ± 0.00	43.15 ± 0.02	**79.17 ± 1.14**
	NMI	35.48 ± 0.44	85.94 ± 1.28	86.91 ± 0.62	38.54 ± 0.87	41.11 ± 0.81	63.45 ± 0.00	70.08 ± 0.27	46.70 ± 0.00	61.53 ± 0.02	**89.12 ± 0.34**
	Purity	15.42 ± 0.55	77.08 ± 2.35	78.37 ± 1.27	16.22 ± 0.65	39.71 ± 1.03	49.75 ± 0.00	57.95 ± 0.80	29.00 ± 0.00	46.80 ± 0.02	**82.23 ± 1.21**
	Fscore	5.12 ± 0.28	70.03 ± 2.69	70.89 ± 1.49	2.59 ± 0.25	26.78 ± 0.60	30.60 ± 2.50	37.99 ± 0.14	10.50 ± 0.00	26.91 ± 0.03	**75.57 ± 0.95**
	Precision	3.01 ± 0.15	65.32 ± 3.31	67.47 ± 1.56	2.27 ± 0.23	23.73 ± 0.68	28.96 ± 0.00	41.15 ± 0.10	8.84 ± 0.00	25.69 ± 0.03	**72.01 ± 0.91**
0.2	ACC	14.83 ± 0.50	75.28 ± 1.08	74.25 ± 2.44	16.22 ± 0.67	27.98 ± 1.31	45.75 ± 0.00	47.88 ± 0.92	28.50 ± 0.00	34.80 ± 0.03	**78.77 ± 1.17**
	NMI	30.94 ± 0.44	86.61 ± 0.76	86.09 ± 1.12	38.10 ± 0.53	48.07 ± 0.76	63.35 ± 0.00	63.48 ± 0.02	47.55 ± 0.00	54.76 ± 0.01	**87.32 ± 0.57**
	Purity	15.07 ± 0.54	78.48 ± 0.95	77.33 ± 1.90	16.88 ± 0.66	29.23 ± 1.18	48.50 ± 0.00	49.63 ± 0.27	31.25 ± 0.00	37.10 ± 0.03	**80.63 ± 0.91**
	Fscore	14.19 ± 0.37	72.19 ± 1.67	69.59 ± 2.13	4.12 ± 0.48	10.90 ± 0.95	30.56 ± 0.00	29.10 ± 0.53	15.22 ± 0.00	17.32 ± 0.00	**72.29 ± 1.07**
	Precision	3.85 ± 0.07	66.74 ± 1.47	65.59 ± 2.41	3.14 ± 0.24	10.25 ± 0.88	28.74 ± 0.00	31.78 ± 0.33	11.68 ± 0.00	16.45 ± 0.00	**68.89 ± 1.28**
0.3	ACC	13.50 ± 0.22	74.10 ± 2.59	74.73 ± 1.43	15.00 ± 0.60	27.95 ± 0.40	53.50 ± 0.00	36.38 ± 0.88	26.00 ± 0.00	34.30 ± 0.00	**78.25 ± 1.32**
	NMI	25.37 ± 0.29	84.90 ± 0.94	84.90 ± 0.84	35.54 ± 0.64	48.74 ± 0.56	68.58 ± 0.00	55.29 ± 0.66	44.58 ± 0.00	54.65 ± 0.00	**86.20 ± 0.40**
	Purity	13.92 ± 0.33	76.92 ± 1.84	76.63 ± 1.23	15.43 ± 0.67	28.93 ± 0.46	55.00 ± 0.00	37.95 ± 0.73	27.75 ± 0.00	37.10 ± 0.01	**80.00 ± 1.25**
	Fscore	29.36 ± 0.15	69.20 ± 2.07	67.51 ± 1.56	4.19 ± 0.48	11.77 ± 0.39	40.33 ± 0.00	17.33 ± 0.16	11.44 ± 0.00	17.32 ± 0.00	**70.51 ± 1.26**
	Precision	4.13 ± 0.02	63.79 ± 2.27	64.11 ± 1.69	2.69 ± 0.48	10.56 ± 0.43	37.41 ± 0.00	19.55 ± 0.34	7.53 ± 0.00	16.45 ± 0.00	**66.23 ± 0.94**
0.4	ACC	11.75 ± 0.42	72.17 ± 2.64	71.73 ± 2.03	14.48 ± 0.53	47.93 ± 1.50	57.75 ± 0.00	27.53 ± 0.40	20.75 ± 0.00	32.10 ± 0.02	**73.28 ± 1.66**
	NMI	18.84 ± 0.13	83.25 ± 1.10	83.23 ± 0.67	32.79 ± 0.67	62.75 ± 0.55	71.24 ± 0.00	48.18 ± 0.70	34.59 ± 0.00	53.32 ± 0.01	**83.42 ± 0.35**
	Purity	12.72 ± 0.14	75.30 ± 1.99	73.60 ± 1.65	14.70 ± 0.44	51.00 ± 1.17	60.25 ± 0.00	28.63 ± 0.74	22.00 ± 0.00	34.20 ± 0.02	**75.62 ± 1.06**
	Fscore	51.69 ± 0.20	**66.57 ± 2.45**	63.97 ± 1.17	8.98 ± 0.31	29.28 ± 1.21	44.44 ± 0.00	9.89 ± 0.58	21.22 ± 0.00	15.40 ± 0.02	65.31 ± 1.07
	Precision	4.28 ± 0.00	60.39 ± 2.68	**60.67 ± 1.64**	3.50 ± 0.00	27.63 ± 0.98	13.71 ± 0.91	13.07 ± 0.79	5.45 ± 0.00	14.79 ± 0.02	58.59 ± 1.13
0.5	ACC	9.25 ± 0.00	72.25 ± 1.37	71.80 ± 2.09	14.50 ± 0.29	59.53 ± 1.07	49.50 ± 0.00	15.38 ± 0.77	20.25 ± 0.00	30.65 ± 0.01	**74.83 ± 1.56**
	NMI	10.02 ± 0.00	82.17 ± 0.84	**82.67 ± 0.91**	29.51 ± 0.38	71.03 ± 0.54	66.97 ± 0.00	32.01 ± 0.52	32.21 ± 0.00	51.25 ± 0.01	82.61 ± 0.73
	Purity	12.25 ± 0.00	74.68 ± 1.17	74.13 ± 1.78	14.75 ± 0.41	61.53 ± 0.82	52.25 ± 0.00	17.40 ± 0.23	20.25 ± 0.00	32.35 ± 0.01	**76.86 ± 1.19**
	Fscore	**80.83 ± 0.00**	**66.08 ± 1.54**	63.55 ± 2.33	20.86 ± 0.13	44.63 ± 0.72	41.89 ± 0.00	4.00 ± 0.26	20.72 ± 0.00	13.03 ± 0.01	65.21 ± 1.08
	Precision	4.38 ± 0.00	61.44 ± 1.71	**59.94 ± 2.16**	4.11 ± 0.00	40.52 ± 1.09	21.58 ± 0.83	8.73 ± 1.35	6.98 ± 0.00	12.33 ± 0.01	57.56 ± 2.73

Table 15. Running time for different clustering algorithms on benchmark datasets.

Dataset	Ours	UEAF	IMSR	T-UMC	MVC-UM	HCLS-CGL	IMSC-AGL	SIMVC	BGVI-MVSC	IMVTSC-MVI
Yale	8.74	7.84	0.60	10.34	5.07	0.20	7.31	2.92	0.34	8.54
YaleA	1.26	0.34	0.30	4.54	0.66	0.13	2.92	1.19	0.42	1.38
BBCSport	20.98	3.83	0.62	40.40	8.42	0.53	26.53	2.66	3.71	20.86
COIL20	217.47	30.16	4.15	756.04	138.16	4.33	280.80	11.91	39.50	188.78
ORL	19.49	9.50	1.80	39.98	13.22	0.72	27.55	3.41	2.71	29.01

4.9. Ablation Study

Compared with existing methods, the proposed model mainly introduces two innovative modules: the dimensionality reduction processing of the original data and the coupling of the cross-view similarity matrices. Therefore, we introduce two degenerate models to verify the effectiveness of the proposed model.

Ablation study on dimensionality reduction: To explore whether the dimensionality reduction processing is useful, we fix $\boldsymbol{P}^v$ as the identity matrix. This degenerate model is called TUIMC-d1.

Ablation study on cross-view coupling: To explore the role of the cross-view coupling matrix $\boldsymbol{T}^v$ in clustering, we fix the coupling matrix $\boldsymbol{T}^v$ as the identity matrix, which means not performing the coupling learning of the similarity matrices of each view. This degenerate model is called TUIMC-d2. TUIMC-d2 is as follows:

$$\begin{aligned} &\min_{\boldsymbol{Z}^v,\boldsymbol{E}^v,\boldsymbol{P}^v,\boldsymbol{B}^v} \lambda_1||\boldsymbol{\mathcal{Z}}||_{\circledast} + \sum_{v=1}^{V}||\boldsymbol{Z}^b - \boldsymbol{Z}^v||_F^2 + \lambda_2||\boldsymbol{E}^v||_{2,1} \\ &s.t. \quad \boldsymbol{P}^{v^\top}\boldsymbol{X}^v + \boldsymbol{B}^v\boldsymbol{W}^v = (\boldsymbol{P}^{v^\top}\boldsymbol{X}^v + \boldsymbol{B}^v\boldsymbol{W}^v)\boldsymbol{Z}^v + \boldsymbol{E}^v, \\ &\boldsymbol{\mathcal{Z}} = \Psi(\boldsymbol{Z}^1, \boldsymbol{Z}^2, \ldots, \boldsymbol{Z}^V), \\ &\boldsymbol{P}^v\boldsymbol{P}^{v^\top} = \boldsymbol{I}. \end{aligned} \tag{38}$$

Analysis of ablation experiment results: The experimental results of the three models on the five datasets with a 30% missing rate are presented in Table 16. The best results are highlighted in bold. Compared with the proposed models, the two degraded models exhibit certain disadvantages across all metrics. For example, on the YaleA dataset, the ACC, NMI, and purity of TUIMC-d1 decrease by 3.53%, 5.89%, and 3.53%, respectively. On the BBCSport dataset, compared with TUIMC, the ACC, NMI, and purity of TUIMC-d2 decrease by 25.06%, 32.61%, and 25.66%, respectively. These results verify the effectiveness of the two components.

Table 16. Ablation experiment results (mean% ± standard deviation%) on five datasets with 30% missing rate.

Model	Metric	YaleA	Yale	BBCSport	ORL	COIL20
TUIMC-d1	ACC	85.86 ± 0.35	65.64 ± 0.70	56.92 ± 0.85	76.58 ± 2.18	75.49 ± 1.56
	NMI	83.50 ± 0.23	67.61 ± 0.59	33.99 ± 1.11	85.81 ± 0.94	84.74 ± 0.54
	Purity	85.86 ± 0.35	66.85 ± 66.85	62.81 ± 0.85	78.58 ± 1.63	77.93 ± 1.62
TUIMC-d2	ACC	60.42 ± 3.41	37.52 ± 2.79	65.66 ± 7.31	68.69 ± 2.11	61.30 ± 1.70
	NMI	68.11 ± 2.99	41.01 ± 2.24	46.30 ± 9.20	73.99 ± 1.10	76.12 ± 1.09
	Purity	61.82 ± 3.32	38.61 ± 2.89	67.17 ± 5.43	69.42 ± 1.81	64.23 ± 1.49
TUIMC	ACC	**89.39 ± 0.32**	**68.48 ± 2.46**	**90.72 ± 0.01**	**78.25 ± 1.32**	**77.01 ± 0.50**
	NMI	**86.33 ± 0.47**	**68.40 ± 1.14**	**78.91 ± 0.61**	**86.20 ± 0.40**	**85.99 ± 0.67**
	Purity	**89.39 ± 0.32**	**68.61 ± 2.35**	**92.83 ± 0.19**	**80.00 ± 1.25**	**79.82 ± 1.38**

4.10. Convergence Study

Experiments are conducted to verify the convergence of the model, and the iterative error curves are analyzed on five datasets. Coupling error1 = $\sum_{v=1}^{V}\frac{1}{V}||\boldsymbol{T}^v - \boldsymbol{M}^v||_\infty$; reconstruction error2 = $\sum_{v=1}^{V}\frac{1}{V}||\boldsymbol{P}^{v^\top}\boldsymbol{X}^v + \boldsymbol{B}^v\boldsymbol{W}^v - \left(\boldsymbol{P}^{v^\top}\boldsymbol{X}^v + \boldsymbol{B}^v\boldsymbol{W}^v\right)\boldsymbol{Z}^v - \boldsymbol{E}^v||_\infty$. The convergence curves of $\log(\text{error1}+1)$ and $\log(\text{error2}+1)$ are plotted, and labeled in red and blue, respectively, as illustrated in Figure 5. The horizontal axis represents the number of iterations, while the vertical axis represents the Error $= \log(\text{error}+1)$. We observe that the reconstruction error decreases rapidly within the first 10 iterations, indicating that the model quickly learns to recover the missing data and couple the views. The coupling error, as shown in Figure 5, also shows a similar trend, dropping sharply in the initial iteration, with a short peak appearing in the tenth iteration, and then gradually stabilizing. This phenomenon occurs because the algorithm is sensitive to the initial values. Overall, the algorithm achieves efficient convergence within 60 iterations.

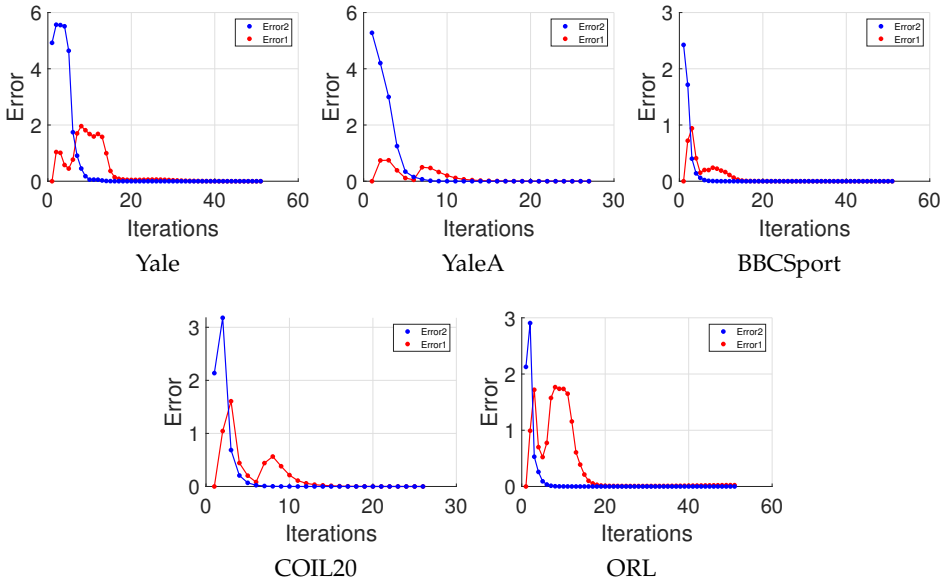

Figure 5. Coupling error curves of $\boldsymbol{T}^v$ and reconstruction error curves of $\boldsymbol{Z}^v$ for 10% miss rate.

5. Conclusions

This paper proposes a novel method named Tensor-based Uncoupled and Incomplete Multi-view Clustering (TUIMC) to address the issues of incomplete and uncoupled multi-view clustering. Through cross-view self-representation coupling, each view is coupled with the template view. The high-order correlations of multi-view data are learned through tensor low-rank approximation based on tensor singular value decomposition (t-SVD). An efficient algorithm is designed to solve the proposed method. Compared with nine advanced models on five datasets, including those for incomplete multi-view clustering methods and uncoupled multi-view clustering methods, TUIMC demonstrates efficient clustering performance.

However, the proposed method has a notable limitation: computational efficiency. Although TUIMC performs remarkably well in handling incomplete and uncoupled views, its matrix inverse operations lead to a significant increase in runtime when dealing with extremely large-scale datasets. Future works will focus on improving the clustering performance, significantly reducing the computational complexity, and exploring the application of this method in large-scale multi-view data.

Author Contributions: Conceptualization, Y.L. and W.G.; methodology, Y.L.; software, Y.L.; writing—original draft preparation, Y.L.; validation, Y.L, W.L. and J.S.; writing—review and editing, Y.L. and W.G.; resources Q.Z. and S.Y.; data curation, Y.L., W.L. and J.S.; visualization, Y.L., Q.Z. and S.Y.; supervision W.G., W.L., J.S., Q.Z. and S.Y. All authors have read and agreed to the published version of the manuscript.

Funding: This work was supported by the Open Fund of Key Laboratory of Cyber-Physical Fusion Intelligent Computing (South Central Minzu University), State Ethnic Affairs Commission (Grant No. CPFIC202303).

Data Availability Statement: The data used to support the findings of the study are available from the first author upon request. The author's email address is pping7349@gmail.com.

Conflicts of Interest: The authors declare that there are no conflicts of interest regarding the publication of this paper.

References

1. Ren, Y.; Chen, X.; Xu, J.; Pu, J.; Huang, Y.; Pu, X.; Zhu, C.; Zhu, X.; Hao, Z.; He, L. A novel federated multi-view clustering method for unaligned and incomplete data fusion. *Inf. Fusion* **2024**, *108*, 102357. [CrossRef]
2. Guo, W.; Che, H.; Leung, M.F. Tensor-Based Adaptive Consensus Graph Learning for Multi-View Clustering. *IEEE Trans. Consum. Electron.* **2024**, *70*, 4767–4784. [CrossRef]
3. Guo, W.; Che, H.; Leung, M.F.; Jin, L.; Wen, S. Robust Mixed-order Graph Learning for incomplete multi-view clustering. *Inf. Fusion* **2025**, *115*, 102776. [CrossRef]
4. Guo, W.; Che, H.; Leung, M.F. High-order consensus graph learning for incomplete multi-view clustering. *Appl. Intell.* **2025**, *55*, 521. [CrossRef]
5. Han, Q.; Hu, L.; Gao, W. Feature relevance and redundancy coefficients for multi-view multi-label feature selection. *Inf. Sci.* **2024**, *652*, 119747. [CrossRef]
6. Hu, X.; Li, Z.; Wu, Y.; Liu, J.; Luo, X.; Ren, J. Neighbouring-slice Guided Multi-View Framework for brain image segmentation. *Neurocomputing* **2024**, *575*, 127315. [CrossRef]
7. Wan, X.; Liu, J.; Gan, X.; Liu, X.; Wang, S.; Wen, Y.; Wan, T.; Zhu, E. One-step multi-view clustering with diverse representation. *IEEE Trans. Neural Netw. Learn. Syst.* **2024**, *36*, 5774–5789. [CrossRef]
8. Che, H.; Pan, B.; Leung, M.F.; Cao, Y.; Yan, Z. Tensor factorization with sparse and graph regularization for fake news detection on social networks. *IEEE Trans. Comput. Soc. Syst.* **2023**, *11*, 4888–4898. [CrossRef]
9. Pan, B.; Li, C.; Che, H.; Leung, M.F.; Yu, K. Low-rank tensor regularized graph fuzzy learning for multi-view data processing. *IEEE Trans. Consum. Electron.* **2023**, *70*, 2925–2938. [CrossRef]
10. Kilmer, M.E.; Braman, K.; Hao, N.; Hoover, R.C. Third-order tensors as operators on matrices: A theoretical and computational framework with applications in imaging. *SIAM J. Matrix Anal. Appl.* **2013**, *34*, 148–172. [CrossRef]
11. Yang, M.S.; Sinaga, K.P. Federated Multi-View K-Means Clustering. *IEEE Trans. Pattern Anal. Mach. Intell.* **2024**, *47*, 2446–2459. [CrossRef] [PubMed]
12. Pu, X.; Che, H.; Pan, B.; Leung, M.F.; Wen, S. Robust weighted low-rank tensor approximation for multiview clustering with mixed noise. *IEEE Trans. Comput. Soc. Syst.* **2023**, *11*, 3268–3285. [CrossRef]
13. Shen, Q.; Zhang, X.; Wang, S.; Li, Y.; Liang, Y.; Chen, Y. Dual Completion Learning for Incomplete Multi-View Clustering. *IEEE Trans. Emerg. Top. Comput. Intell.* **2024**, *9*, 455–467. [CrossRef]
14. Hu, M.; Chen, S. Doubly aligned incomplete multi-view clustering. In Proceedings of the 27th International Joint Conference on Artificial Intelligence, Stockholm, Sweden, 13–19 July 2018; pp. 2262–2268.
15. Yu, H.; Tang, J.; Wang, G.; Gao, X. A novel multi-view clustering method for unknown mapping relationships between cross-view samples. In Proceedings of the 27th ACM SIGKDD Conference on Knowledge Discovery & Data Mining, Virtual, 14–18 August 2021; pp. 2075–2083.
16. Lin, J.Q.; Chen, M.S.; Wang, C.D.; Zhang, H. A tensor approach for uncoupled multiview clustering. *IEEE Trans. Cybern.* **2022**, *54*, 1236–1249. [CrossRef]
17. Lin, J.Q.; Li, X.L.; Chen, M.S.; Wang, C.D.; Zhang, H. Incomplete Data Meets Uncoupled Case: A Challenging Task of Multiview Clustering. *IEEE Trans. Neural Netw. Learn. Syst.* **2024**, *35*, 8097–8110. [CrossRef]
18. Lin, Z.; Liu, R.; Su, Z. Linearized alternating direction method with adaptive penalty for low-rank representation. *Adv. Neural Inf. Process. Syst.* **2011**, *24*, 612–620.
19. Wang, Y.; Wu, L.; Lin, X.; Gao, J. Multiview spectral clustering via structured low-rank matrix factorization. *IEEE Trans. Neural Netw. Learn. Syst.* **2018**, *29*, 4833–4843. [CrossRef]
20. Zhong, G.; Pun, C.M. Simultaneous Laplacian embedding and subspace clustering for incomplete multi-view data. *Knowl.-Based Syst.* **2023**, *262*, 110244. [CrossRef]
21. Wang, S.; Li, C.; Li, Y.; Yuan, Y.; Wang, G. Self-supervised information bottleneck for deep multi-view subspace clustering. *IEEE Trans. Image Process.* **2023**, *32*, 1555–1567. [CrossRef]
22. Guan, R.; Li, Z.; Tu, W.; Wang, J.; Liu, Y.; Li, X.; Tang, C.; Feng, R. Contrastive multi-view subspace clustering of hyperspectral images based on graph convolutional networks. *IEEE Trans. Geosci. Remote Sens.* **2024**, *62*, 5510514. [CrossRef]
23. Mu, J.; Song, P.; Yu, Y.; Zheng, W. Tensor-based consensus learning for incomplete multi-view clustering. *Expert Syst. Appl.* **2023**, *234*, 121013. [CrossRef]
24. Han, X.; Ren, Z.; Zou, C.; You, X. Incomplete multi-view subspace clustering based on missing-sample recovering and structural information learning. *Expert Syst. Appl.* **2022**, *208*, 118165. [CrossRef]
25. Sinaga, K.P. Bi-Level Multi-View fuzzy Clustering with Exponential Distance. *arXiv* **2025**, arXiv:2503.22932.
26. Sinaga, K.P. Rectified Gaussian kernel multi-view k-means clustering. *arXiv* **2024**, arXiv:2405.05619.
27. Wen, J.; Zhang, Z.; Zhang, Z.; Zhu, L.; Fei, L.; Zhang, B.; Xu, Y. Unified tensor framework for incomplete multi-view clustering and missing-view inferring. In Proceedings of the AAAI Conference on Artificial Intelligence 2021, Virtual, 2–9 February 2021; Volume 35, pp. 10273–10281.

28. Zhong, Q.; Lyu, G.; Yang, Z. Align while fusion: A generalized nonaligned multiview multilabel classification method. *IEEE Trans. Neural Netw. Learn. Syst.* **2024**, *36*, 7627–7636. [CrossRef] [PubMed]
29. Wang, S.; Liu, X.; Zhu, E.; Tang, C.; Liu, J.; Hu, J.; Xia, J.; Yin, J. Multi-view clustering via late fusion alignment maximization. In Proceedings of the IJCAI 2019, Macao, China, 10–16 August 2019; pp. 3778–3784.
30. Liu, G.; Lin, Z.; Yan, S.; Sun, J.; Yu, Y.; Ma, Y. Robust Recovery of Subspace Structures by Low-Rank Representation. *IEEE Trans. Pattern Anal. Mach. Intell.* **2013**, *35*, 171–184. [CrossRef]
31. Fang, X.; Hu, Y.; Zhou, P.; Wu, D.O. Unbalanced incomplete multi-view clustering via the scheme of view evolution: Weak views are meat; strong views do eat. *IEEE Trans. Emerg. Top. Comput. Intell.* **2021**, *6*, 913–927. [CrossRef]
32. Wen, J.; Liu, C.; Xu, G.; Wu, Z.; Huang, C.; Fei, L.; Xu, Y. Highly confident local structure based consensus graph learning for incomplete multi-view clustering. In Proceedings of the IEEE/CVF Conference on Computer Vision and Pattern Recognition 2023, Vancouver, BC, Canada, 17–24 June 2023; pp. 15712–15721.
33. Wen, J.; Zhang, Z.; Xu, Y.; Zhang, B.; Fei, L.; Liu, H. Unified embedding alignment with missing views inferring for incomplete multi-view clustering. In Proceedings of the AAAI Conference on Artificial Intelligence 2019, Honolulu, HI, USA, 27 January–1 February 2019; Volume 33, pp. 5393–5400.
34. Wen, J.; Xu, Y.; Liu, H. Incomplete multiview spectral clustering with adaptive graph learning. *IEEE Trans. Cybern.* **2018**, *50*, 1418–1429. [CrossRef]
35. Sun, L.; Wen, J.; Liu, C.; Fei, L.; Li, L. Balance guided incomplete multi-view spectral clustering. *Neural Netw.* **2023**, *166*, 260–272. [CrossRef]
36. Liu, J.; Liu, X.; Zhang, Y.; Zhang, P.; Tu, W.; Wang, S.; Zhou, S.; Liang, W.; Wang, S.; Yang, Y. Self-representation subspace clustering for incomplete multi-view data. In Proceedings of the 29th ACM International Conference on Multimedia, Virtual, 20–24 October 2021, pp. 2726–2734.
37. Wen, Y.; Wang, S.; Liang, K.; Liang, W.; Wan, X.; tLiu, X.; Liu, S.; Liu, J.; Zhu, E. Scalable Incomplete Multi-View Clustering with Structure Alignment. In Proceedings of the 31st ACM International Conference on Multimedia, Ottawa, ON, Canada, 29 October–3 November 2023; pp. 3031–3040.
38. Yang, B.; Song, P.; Cheng, Y.; Liu, Z.; Yu, Y. Label completion based concept factorization for incomplete multi-view clustering. *Knowl.-Based Syst.* **2025**, *310*, 112953. [CrossRef]